STRUCTURAL, GEOCHRONOLOGICAL AND METAMORPHIC INVESTIGATION OF THE NORTH TEA LAKE MYLONITE ZONE: A LATE EXTENSIONAL FEATURE WITHIN THE CENTRAL GNEISS BELT, GRENVILLE PROVINCE, ALGONQUIN PARK, ONTARIO.

Laura Ratcliffe

Submitted in partial fulfillment of the requirements
for the degree of Bachelor of Science, Honours
Department of Earth Science
Dalhousie University, Halifax, Nova Scotia
March 2011

Distribution License

DalSpace requires agreement to this non-exclusive distribution license before your item can appear on DalSpace.

NON-EXCLUSIVE DISTRIBUTION LICENSE

You (the author(s) or copyright owner) grant to Dalhousie University the non-exclusive right to reproduce and distribute your submission worldwide in any medium.

You agree that Dalhousie University may, without changing the content, reformat the submission for the purpose of preservation.

You also agree that Dalhousie University may keep more than one copy of this submission for purposes of security, back-up and preservation.

You agree that the submission is your original work, and that you have the right to grant the rights contained in this license. You also agree that your submission does not, to the best of your knowledge, infringe upon anyone's copyright.

If the submission contains material for which you do not hold copyright, you agree that you have obtained the unrestricted permission of the copyright owner to grant Dalhousie University the rights required by this license, and that such third-party owned material is clearly identified and acknowledged within the text or content of the submission.

If the submission is based upon work that has been sponsored or supported by an agency or organization other than Dalhousie University, you assert that you have fulfilled any right of review or other obligations required by such contract or agreement.

Dalhousie University will clearly identify your name(s) as the author(s) or owner(s) of the submission, and will not make any alteration to the content of the files that you have submitted.

If you have questions regarding this license please contact the repository manager at dalspace@dal.ca.

Grant the distribution license by signing and dating below.

_____ _____

Name of signatory Date

DALHOUSIE UNIVERSITY
Inspiring Minds

Department of Earth Sciences
Halifax, Nova Scotia
Canada B3H 4J1
(902) 494-2358
FAX (902) 494-6889

DATE: APRIL 25, 2011

AUTHOR: LAURA M. RATCLIFFE

TITLE: STRUCTURAL, GEOCHRONOLOGICAL AND METAMORPHIC INVESTIGATION OF THE NORTH TEA LAKE MYLONITE ZONE: A LATE EXTENSIONAL FEATURE WITHIN THE CENTRAL GNEISS BELT, GRENVILLE PROVINCE, ALGONQUIN PARK, ONTARIO

Degree: B.Sc. Honours Convocation: MAY Year: 2011

ABSTRACT

The Central Gneiss Belt (CGB) in the western Grenville Province of the Grenville orogen (~1190 – 980 Ma) in southern Ontario exposes a Himalayan scale mountain belt at deep levels. The recently identified North Tea Lake mylonite zone (NTLMZ) is a late, extensional, greenschist facies mylonite zone lying conformably within an amphibolite facies nappe-bounding thrust sense North Tea Lake shear zone (NTLSZ) which separates the Kiosk and Bonfield domains within the western CGB.

Detailed mapping of a transect across the NTLMZ shows lithological and structural variations within the shear zone. The NTLMZ has normal-sense shear determined from microstructural kinematic indicators and extension direction determined from orientation of rotated fold hinges to the down dip direction.

A temperature estimate at the time of mylonitization is based on 1) identification of dynamic recrystallisation processes in quartz and feldspar (400-500 º C), 2) a mineral assemblage suggestive of greenschist facies conditions (300-500 º C) and 3) Electron Backscatter Diffraction (EBSD) analysis indicating the dominant slip system active in quartz (basal <a>, 300-400 º C).

An $^{40}Ar/^{39}Ar$ geochronology investigation of bulk rock samples and mineral separates produced a reliable cooling age of hornblende to be 1025 ±19 Ma. A model assuming a hornblende closure temperature of 500 º C and cooling rate of 2 º C Myr^{-1} suggests a NTLMZ age of ~ 955 – 975 Ma. This age range suggests the NTLMZ was a late Grenville process.

In the extensional NTLMZ the footwall is brought closer to the surface indicating exhumation of the study area, while PT changes from the earlier amphibolite facies NTLSZ to the later green schist facies NTLMZ indicates cooling of the study area. Therefore the NTLMZ suggests cooling and exhumation during late Grenville processes.

TABLE OF CONTENTS

TABLE OF FIGURES

TABLE OF TABLES

Acknowledgements

I would like to thank the faculty and staff of Dalhousie University's Earth Science Department for years of dedicated instruction and support, and the invaluable assistance of Peter Regan and John Foster in the field, Jeff Marsh and Chris Gerbi with EBSD interpretation, and Keith Taylor and Pete Reynolds with the Dalhousie University argon geochron. In addition, I would like to thank Dan MacDonald and Gordon Brown with Dalhousie University's EMP and thin section preparation labs and Thomas Duffet for technical assistance. I am deeply grateful to Becky Jamieson for encouragement and sage advice, Kyle Landry, the Dawson society, and the Dalhousie Earth Science honours class of 2011 for support and motivation. Finally, to my supervisor Nick Culshaw for his guidance and expertise, and for the opportunity to work on some of Canada's most interesting and challenging, geology.

CHAPTER 1: INTRODUCTION

1.1 Introduction to the problem

The Grenville province (Fig 1.1), is the youngest component of the Canadian Shield, it was formed during the 1190 – 980 Ma Grenville orogeny and exposes the doubly thickened crust at middle to lower levels providing a unique opportunity to study a Himalayan-scale orogen at depth. The Grenville province is divided into 1) the Grenville Front Tectonic Zone (GFTZ) the youngest of the zones and bounding the province to the northwest; 2) the Central Gneiss Belt (CGB), comprised of parautochthonous and allochthonous lithologically distinct high grade ductile nappes (domains) of the Laurentian craton (pre-1400 Ma) stacked together with offshore Laurentian supracrustal sequences at deep levels during collision; 3) the Central Metasedimentary Belt (CMB) is composed of allochthonous post-1400 Ma magmatic arcs and marginal basins (Culshaw et. al 1997; Culshaw 2010; Carr et al. 2000).

This study focuses on rocks within the CGB which, in the Algonquin Park region, are subdivided into stacked domains (Fig 1.1) from the base to top: Bonfield, Kiosk, Algonquin (McRaney, Novar, McLintock sub-domains) and Opeongo (Carr et al. 2000; Culshaw 2010). The Bonfield domain consists of granitoid plutons and varied quartzofeldspathic gneiss metamorphosed at amphibolite facies. The dominant feature of this domain is the Bonfield batholith accompanied by smaller granitoid plutons. The Kiosk domain is predominantly granulite facies orthogneiss with a strong SSE inclined gneissic fabric. The North Tea Lake Shear Zone (NTLSZ) lies between the Kiosk and Bonfield domains. It is characterized by fine-grained, highly attenuated banded gneiss with a SE-dipping fabric overprinting an earlier fabric. The shear zone is approximately 3 km with a thrust shear sense (McLeish 2008).

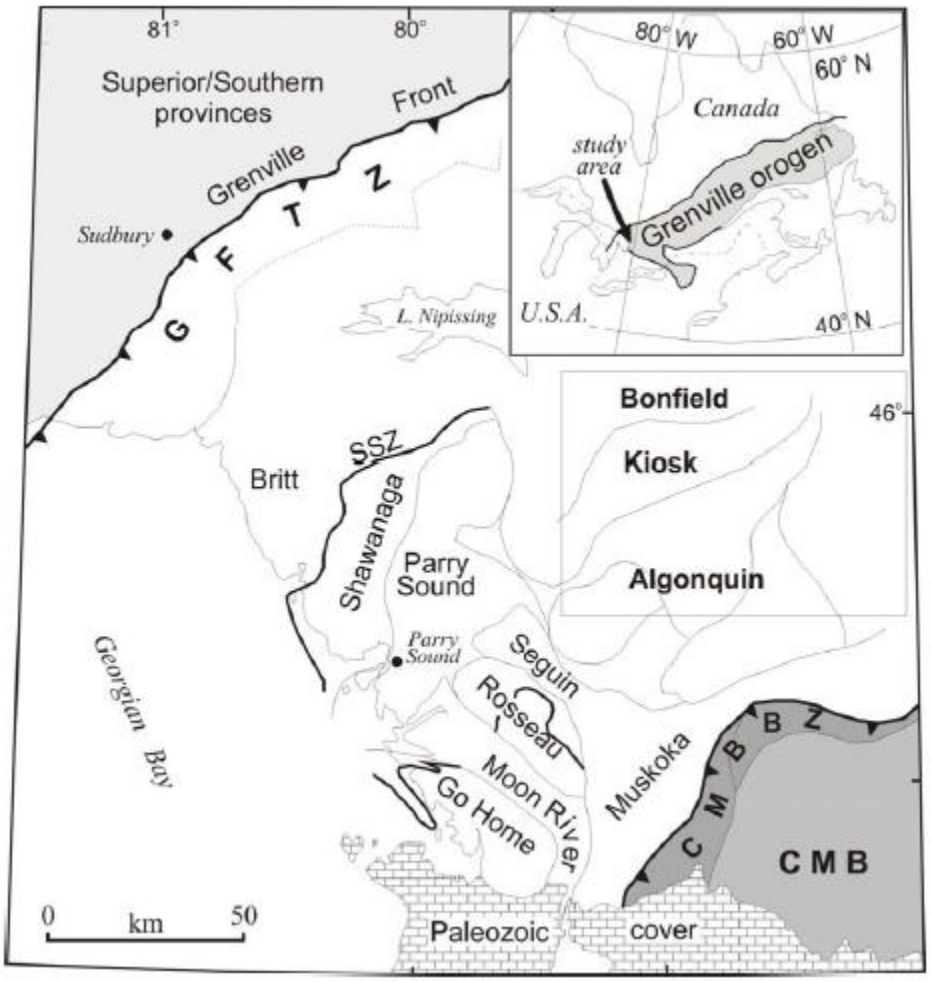

Figure 1.1: Map of Grenville Province showing locations of: 1) Grenville orogen (top right map inset), 2) GFTZ (top left), 3) CGB white area across centre of map, 4) CMB (bottom right), 5) Bonfield and Kiosk domains separated by a line which is the NTLSZ. Figure from Culshaw 2010.

Reconnaissance work done in 2007 (McLeish 2008) identified two locations of mylonite in the eastern arm of North Tea Lake, within the NTLSZ (Fig 1.2). The mylonite is anomalous with respect to the NTLSZ fabric (and very unusual within the CGB) and so was identified as a feature requiring further study. The eastern mylonite location is the focus of this study.

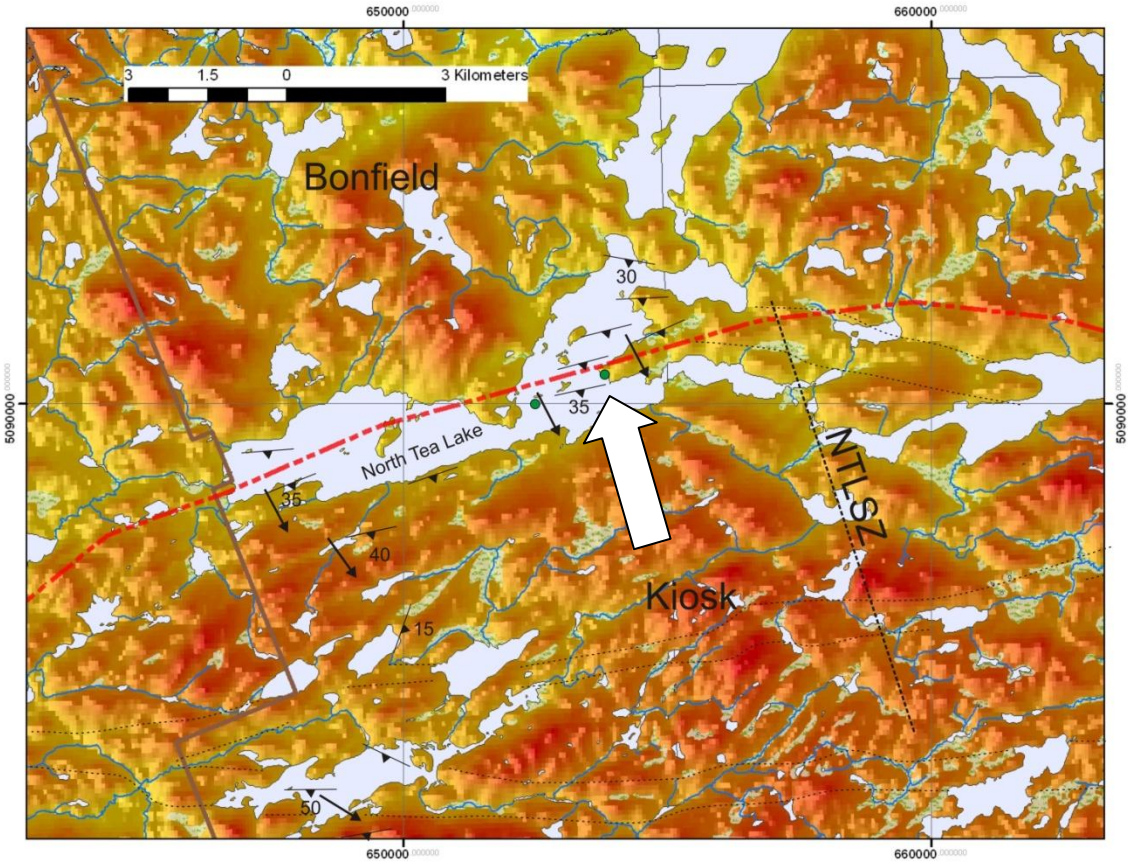

Figure 1.2: Digital Elevation Map of study area. Green circles in the eastern arm of North Tea Lake mark the locations of mylonite, the study area is the green circle marked by the white arrow. The study area is within the NTLSZ which trend is marked by the red line and thickness is marked by the black line. Map compiled by Dr. Nicholas Culshaw.

1.2 Mapping Expedition

This project began with a two week expedition in northwestern Algonquin Park, Ontario, August 6-19th, 2010. The study area, on the east arm of North Tea Lake, is accessible by a one day canoe paddle and portage from Algonquin Park access point # 1. A campsite is conveniently located at the best exposure of the study area and was designated base camp for the group.

The purpose of this expedition was to collect more detailed information on a regional scale shear zone and the mylonite within it, identified by reconnaissance mapping done by

Culshaw and McLeish in 2007 (McLeish 2008). Participants included Dr. Nicholas Culshaw, John Foster, Laura Ratcliffe, and Peter Regan. John Foster investigated the NTLSZ bounding the Kiosk and Bonfield domains as part of a MSc. project concurrently with this study of the NTLMZ. Peter Regan assisted with the investigations while Dr. Culshaw oversaw and advised the students.

1.3 *Study Objectives and Methods of Investigation*

The goal of this study is to characterize the North Tea Lake Mylonite Zone (NTLMZ) in terms of kinematics, structural development, age and the PT conditions of the deformation.

Techniques employed to investigate these objectives include field observations, petrographic study of the mineral assemblage, optical observations of microstructure, including dynamic recrystallisation mechanisms and kinematics, EBSD analysis of quartz lattice preferred orientations, and ^{40}Ar / ^{39}Ar geochronology (step-heating of biotite, hornblende and K-feldspar separates and bulk rock samples).

CHAPTER 2: FIELD RELATIONSHIPS

2.1 General Statement

The goal of the field component of this study was to gather information to determine the structure and kinematics of the NTLMZ and its relationship with the NTLSZ. This was accomplished by detailed mapping of a transect across NTLMZ and collection of samples to be further analyzed in the laboratory.

2.2 Mapping Methods

A detailed map was developed showing the location of each unit identified and its relationship to the surrounding area. In order for the map to be as accurate as possible a baseline (Fig. 2.1) with a known orientation was set along the outcrop. All samples, structural measurements (e.g. foliations, folds limbs) and boundary locations were referenced to this base line. Peter Regan developed a sketch of the outcrop outlines along the baseline which is used as the foundation of the map. Rope marked with metre increments was used to mark the base line. Each 11 m section was assigned a baseline identification number for sample reference. The sections are 11 m each simply because this is the length of the rope that was available. The map created in the field was then transposed to Adobe Illustrator. A summary of the map showing the outcrops and the lithological and structural-textural boundaries of units is shown in Fig. 2.3. Two map inserts with structural information and sample locations can be referenced in the back cover for more detailed results of the mapping project.

Figure 2.1: Baseline on a mylonitized migmatite. Flagging tape marks metre increments. Samples locations were then measured by the distance perpendicular to the baseline.

2.2.1 Sample Collection

The samples are from locations representative of each unit along the transect. The samples were oriented and numbered with reference to the baseline section number and then alphabetically named in the order it was collected from each baseline. (See map insert "Sample Location Map" in back flap of thesis)

2.2.2 Structural Methods

The orientations of penetrative foliations and metre-scale folds were measured in the field. To better determine the geometry of folds, measurements of limb attitudes and axial traces were collected. These were then plotted on a stereonet and the orientation of the hinges determined. One hand sample collected in the field contains a small fold (~10 cm) which was cut with a saw to reveal the relationship between the axial planar foliation and the hinge line.

2.3 Observations

The NTLMZ outcrops in two locations in the east arm of North Tea Lake. This study focuses on the location with the best exposure on the eastern peninsula of North Tea Lake (Fig 2.2). The study area covers a 115 m transect of the NTLMZ along the shoreline located within the green box in Figure 2.2. The outcrops are bounded by the lake to the east and vegetation to the west. The maximum elevation difference is about 40 ft on the northern section of the study area, this is due to a ridge that creates steep cliffs (Fig. 2.4). The ridge slopes to the southeast so the elevation difference decreases 20 ft in the centre of the transect. The southern section of the transect is relatively flat with an elevation difference of 10 ft throughout. The map (Fig. 2.3) of this study area runs northwest to southeast and therefore transects all exposed units of the shear zone and the NTLMZ host rock, which bounds the northern and southern ends of the transect. A section of the transect is shown in Fig. 2.4, this figure illustrates the relationship between units as shown in Fig. 2.3.

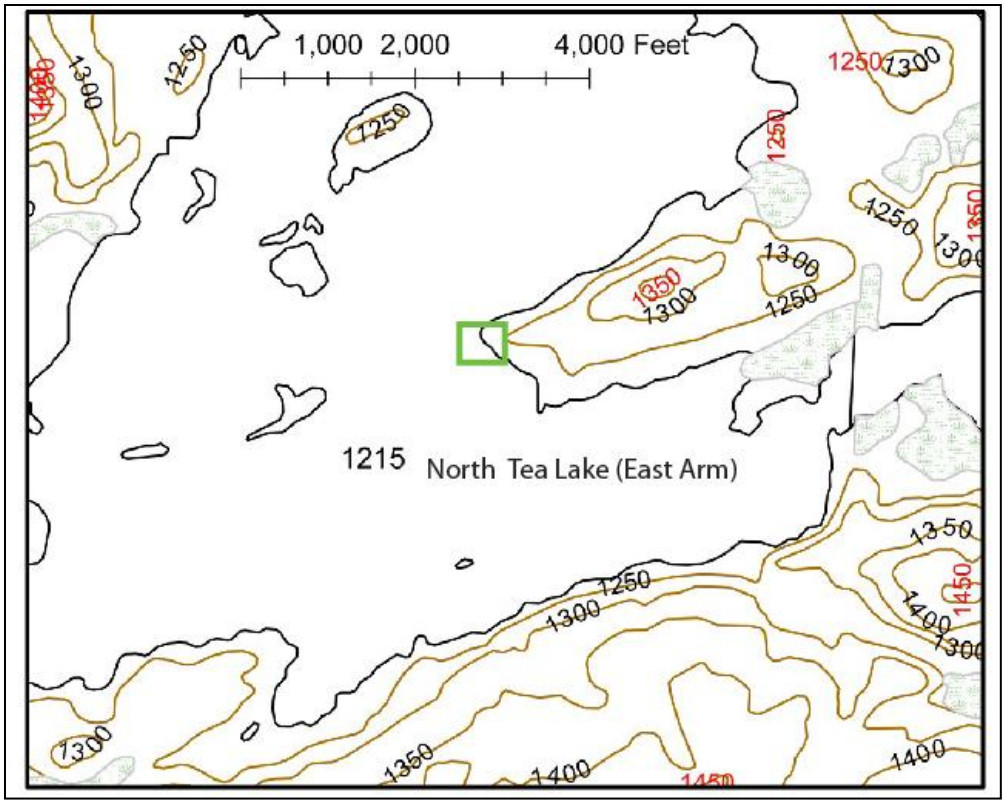

Figure 2.2 Topographic map showing location of study area and nearby elevations (in feet), the study area is about 370 ft wide and lies within the green square. Note the steep topography (marked by the 1250 ft elevation contours) trending into the northeastern portion of the study area.

The map (Fig. 2.3) shows the relationship between the lithological and structural-textural units of the NTLMZ. The lithological boundaries indicate compositional changes between the units. The NTLMZ is primarily composed of two compositionally distinct protoliths, these are tonalitic gneiss and granitoid migmatite. More highly strained portions of these units form different textural and structural units which are defined in Fig. 2.3 by the gradational textural-structural boundary. The tonalitic straight gneiss, folded gneiss, and gneiss enclaves are all of a tonalitic composition but have different structural-textural characteristics. Likewise, the weakly to strongly mylonitized and locally folded migmatite and the protolith migmatite are all of the same composition but are classified into different units by their structural-textural differences.

The granitic straight gneiss and mafic pod are lithologically distinct with no textural-structural counterpart.

The structural and textural boundaries define the location of the NTLMZ within the study area. The northern boundary of the NTLMZ is defined by the lower migmatite (host rock) and the upper weakly mylonitized folded migmatite (NTLMZ) shown in Fig. 2.3: Baseline 1.2 & 2.1. The southern boundary of the NTLSZ is defined by the lower mylonitized migmatite (NTLSZ) and the upper granitic straight gneiss (host rock), shown in Fig. 2.3: Baseline 3.5. The units of NTLMZ are stacked as a folded mylonitized migmatite and gneiss (Fig. 2.3: Baselines 2.1& 2.2), overlain by a heterogeneous layer of strained migmatite (Fig. 2.3: Baselines 2.2-3.5). The mylonitized migmatite contains lithologically distinct gneiss enclaves and a mafic pod indicated by a lithological boundary.

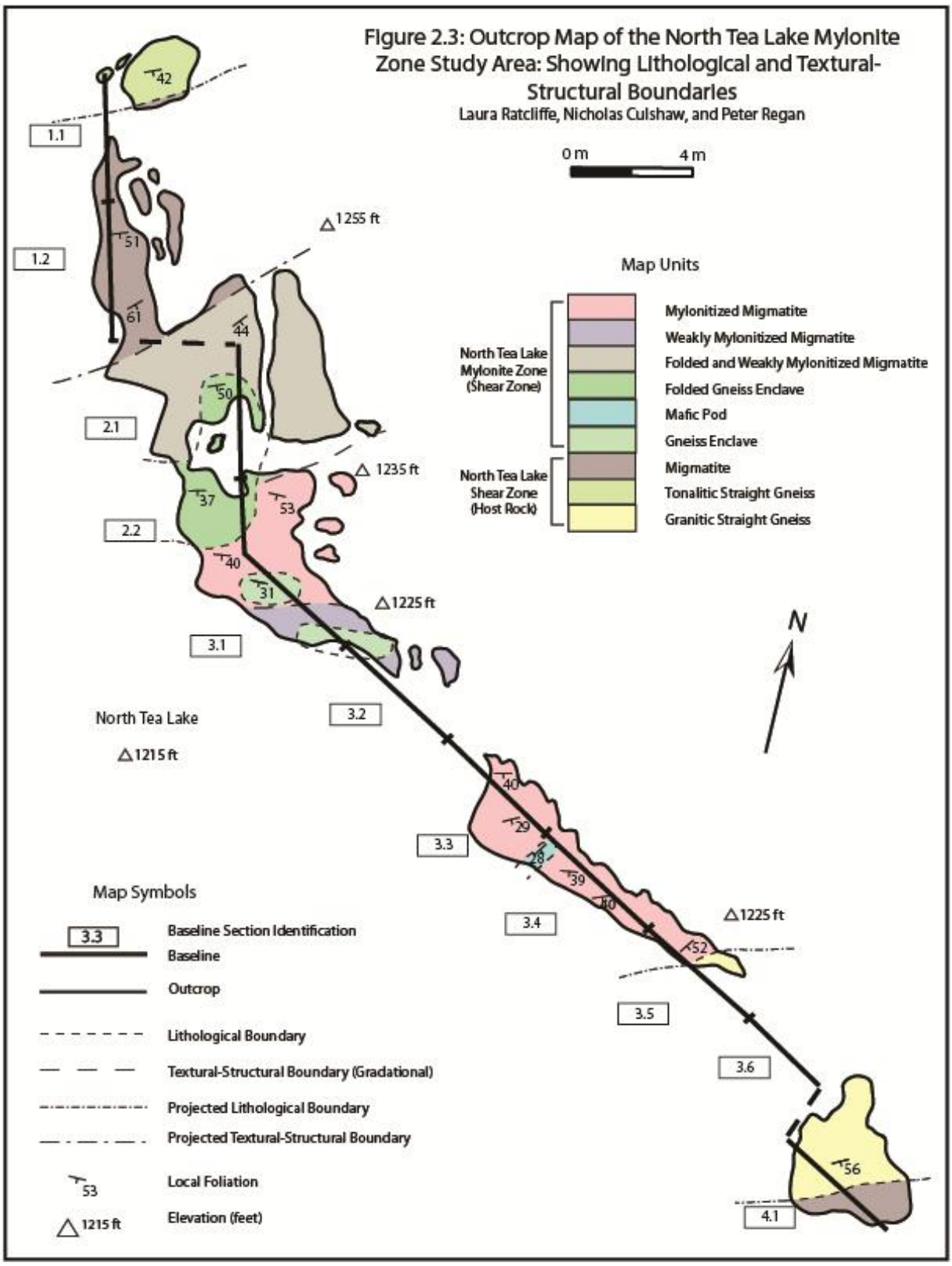

Figure 2.3: Outcrop Map showing a 115 m transect of the North Tea Lake Mylonite Zone. The transect is bounded by a lake to the west and lack of exposure to the east. The maximum elevation change is 40 ft. For larger more detailed maps see inserts in flap at the back of thesis.

Figure 2.4: Photograph of outcrop in northern half of transect. The short dashed lines represent changes in lithology while the long dashed lines show gradational changes in mylonitization of the migmatite. Note the gneiss enclave which is lower in the section than the surrounding mylonite. This figure also demonstrates the relationship between the SE dipping units such as the folded protomylonite migmatite and the overlying mylonitized migmatite.

2.3.1 Tonalitic Straight Gneiss

The tonalitic straight gneiss is the lowest unit bounding the study area and host rock of the NTLMZ, (Fig. 2.3: Baseline 1.1). The outcrop is dominated by a large isoclinal fold (3 x 1.5 m) of strongly layered tonalitic (quartz and plagioclase rich) gneiss. The tonalitic gneiss contains some biotite/hornblende rich bands.

2.3.2 Migmatite

The migmatite unit (Fig. 2.3: Baseline 1.1-1.2, &4.1) is the protolith of the mylonitized migmatite which defines the North Tea Lake shear zone. The first occurrence of migmatite overlies the tonalitic straight gneiss in the northernmost outcrop. The migmatitic granitoid - contains bands of pink leucosomes within a plagioclase-quartz rich (tonalitic) matrix. The leucosome is primarily potassium feldspar and quartz (1-3mm grains), while the darker bands contain more biotite, plagioclase and quartz of a smaller grain size (0.5 mm). The migmatite contains characteristic hornblende porphyroblasts (1-5 mm) which are present throughout the migmatite in varying concentrations. Outside the NTLMZ the migmatite is relatively straight with a foliation dipping about 50º to the southeast.

2.3.3 Weakly Mylonitized Folded Migmatite

The weakly mylonitized folded migmatite (Fig. 2.5) unit overlies the protolith migmatite (Fig. 2.3: Baseline 2.1). The gneissic banding between the leucosome and tonalitic layers is more defined then in the protolith and the grain size of the leucosomes is reduced (0.5-1 mm) suggesting it has been weakly mylonitized. The boundaries of this unit are gradational, the grain size coarsens towards the lower migmatite unit and fines towards the overriding mylonite unit.

Figure 2.5: Weakly Mylonitized Folded Migmatite: a) Fold from plan view looking down axial trace (60 cm board for scale). b) Folded protomylonite migmatite overlying straight migmatite layer on cliff face (pencil for scale).

2.3.4 Folded Gneiss Enclave

A pod of folded tonalitic straight gneiss (Fig 2.6) is found between the weakly mylonitized folded migmatite and the overlying mylonitized migmatite (Fig. 2.3: Baseline 2.1 & 2.2). The boundaries of the folded gneiss and surrounding units suggest this unit is an enclave because the enclave does not extend across the outcrop (see 3 point junction of boundaries (Fig 2.3: Baseline 2.2)). The geometry of the folds in the gneiss enclave is similar to those of the folded mylonitized migmatite. The similar fold structure to that of the folded migmatite suggests a similar style of deformation related to the mylonitization event.

It is probable that this folded gneiss originated as an enclave of tonalitic straight gneiss within the migmatite. The gneiss is composed of banded biotite rich and tonalitic layers. The grain size is (0.5 to 1 mm).

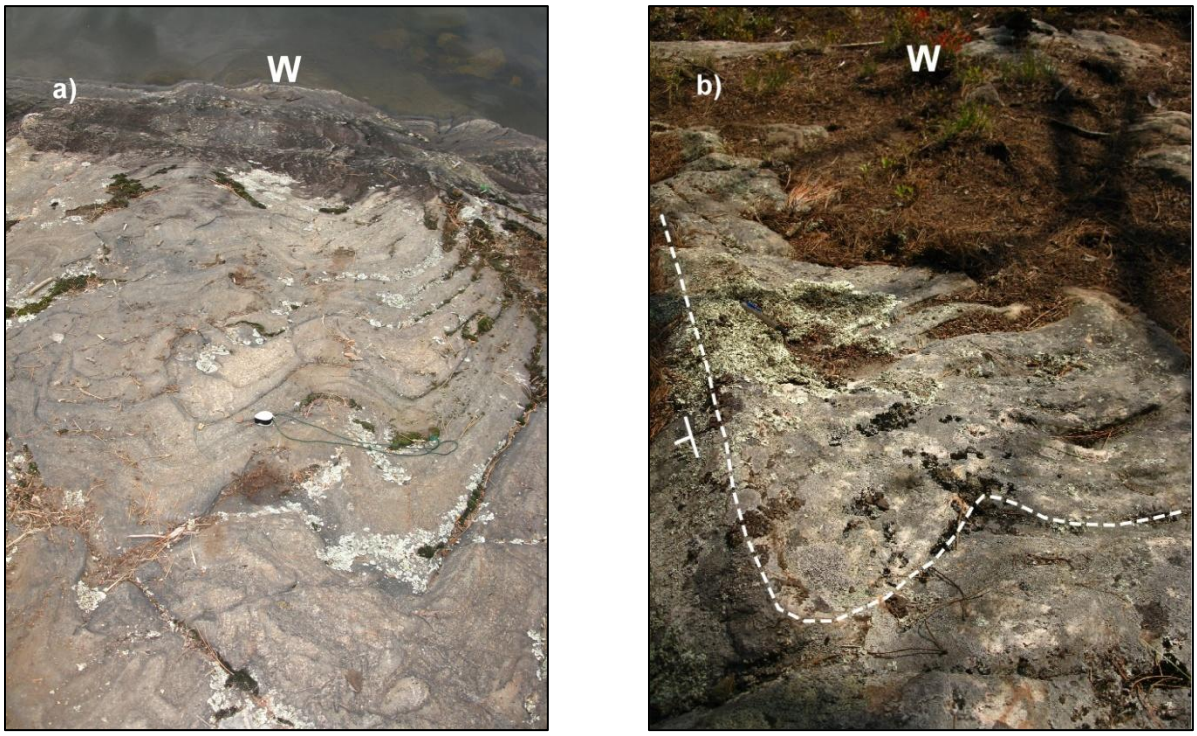

Figure 2.6: a) Folded Gneiss (hand lens for scale), b) Folded Gneiss (pencil for scale) with fold trace marked by dashed line. Strike and dip symbol shows southern limb joining the dominant foliation of shear zone (077/39 SE).

2.3.5 Mylonitized Migmatite

There are several units of mylonitized migmatite. The mylonitization of the migmatite is heterogeneous across the shear zone, and grades between weakly to strongly mylonitized migmatite (Fig. 2.3: Baselines 3.1-3.4). The folded migmatite (Fig. 2.3: Baseline 2.1) is also weakly mylonitized and marks the lowest unit of the NTLMZ. The strongest mylonitized migmatite unit occurs at baseline 3.3 and 3.4, and the western portion of baseline 3.1 (Fig. 2.3). The strain heterogeneity produces a weakly mylonitized migmatite (Fig. 2.3: Baselines 3.1& 3.2) between the stronger mylonitized units. The mylonite consists of strongly foliated very fine-grained bands of leucosome and grey bands (Fig. 2.1) dipping to the southeast. There is no

obvious lineation but elongated feldspar (4-6 mm) and hornblende (1-3 mm) porphyroclasts are visible and show elongated tails perpendicular the strike of the foliation.

2.3.6 Gneiss Enclaves

There are two tonalitic gneiss enclaves in the mylonitized migmatite (Fig. 2.3: Baselines 3.1 & 3.2). These enclaves are composed of tonalitic banded gneiss very similar to that of the tonalitic straight gneiss described in section *2.3.1*. The northern enclave (labelled Gneiss Enclave in Fig. 2.4) is surrounded by a mylonitized migmatite and located in a lower unit then the mylonitized migmatite but is made visible by an eroded section of the mylonite. The second enclave is 2 m southeast (Fig .2.3: Baseline 3.2).

The relationship between the two enclaves is unclear but it is probable the enclaves are two exposed sections of the same unit which is separated by the mylonitized migmatite.

2.3.7 Mafic Pod

A mafic pod (Fig. 2.7.a) is present within the southernmost mylonite unit (Fig 2.3: Baseline 3.4). The pod dip is concordant with the surrounding foliation. The mafic pod is composed primarily of hornblende and biotite with 10% feldspar. The grains are 1-2 mm.

This pod is also thought to have been present in the protolith migmatite, and then mylonitized with the rest of the shear zone.

2.3.8 Granitic Straight Gneiss

The unit overlying the mylonitized migmatite is granitic straight gneiss (Fig 2.7.b.). This unit is the upper host rock unit bounding the NTLMZ (Fig. 2.3: Baseline 4.1). The outcrop contains a large isoclinal fold. The granitic gneiss is fine grained (0.1-1mm) pink potassium-feldspar rich layers banded with thinner dark layers.

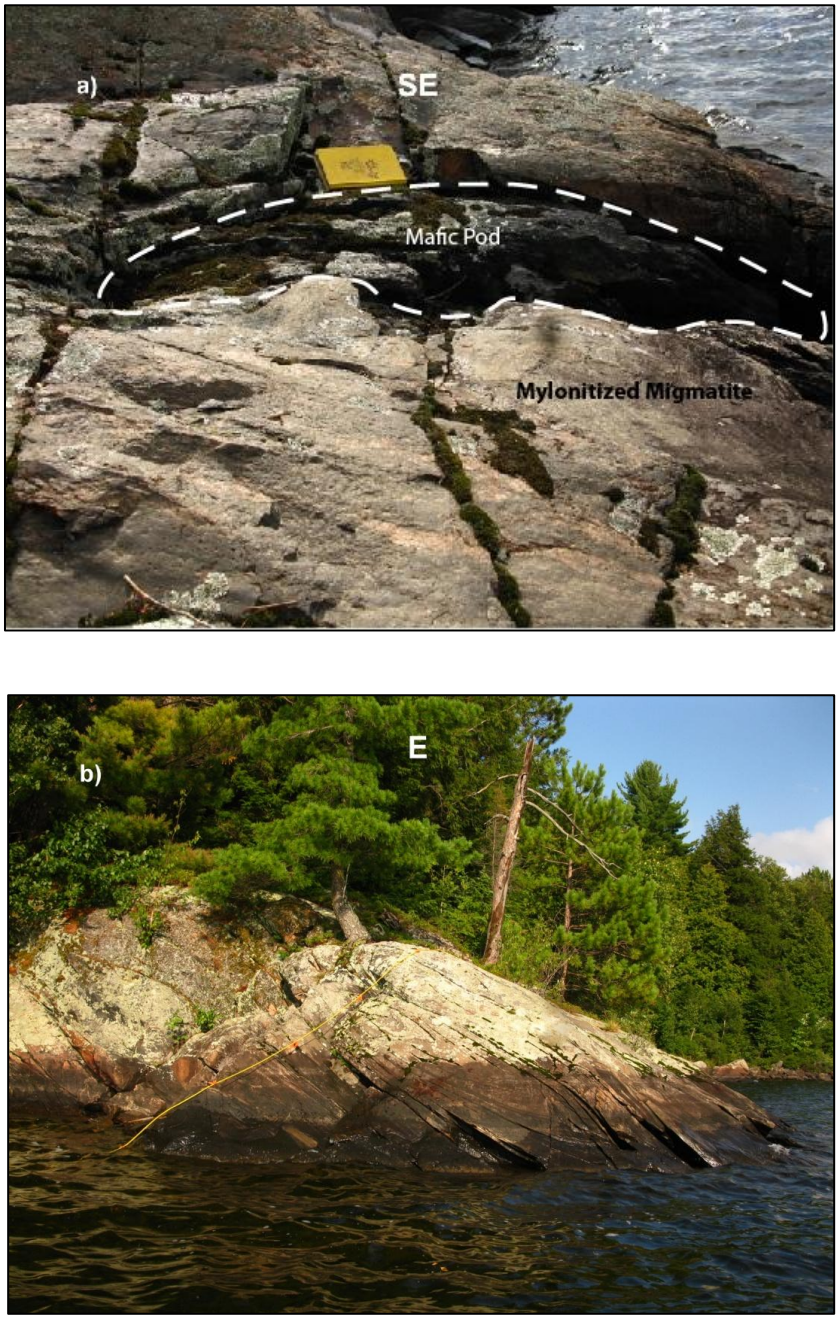

Figure 2.7: Outcrop photographs: a) Mafic Pod in mylonitized migmatite dipping southeast, b) Granitic Straight Gneiss isoclinals fold marking southern boundary of North Tea Lake shear zone.

2.4 Structural Observations

The NTLMZ is dominated by a southeast dipping mylonitic foliation (Fig. 2.8.b) yet there is no obvious lineation. It is difficult to observe aligned hornblende porphyroclasts but observation of cut foliation surfaces suggest there is an alignment present. The gneissic foliation of the NTLSZ is the same as the mylonitic foliation of the NTLMZ (Fig. 2.8.b). Folds were located in two units described in section *2.3.3 and 2.3.4*, including a weakly mylonitized folded migmatite (Fig. 2.5), and a folded gneiss enclave (Fig. 2.6).

The stereonet in Fig 2.8.a shows the poles to fold limbs from eight folds located in these units. The average profile plane dips to the northwest. The hinge as determined from the average profile plane to plunges to the southeast close to the dip direction of the average mylonitic foliation.

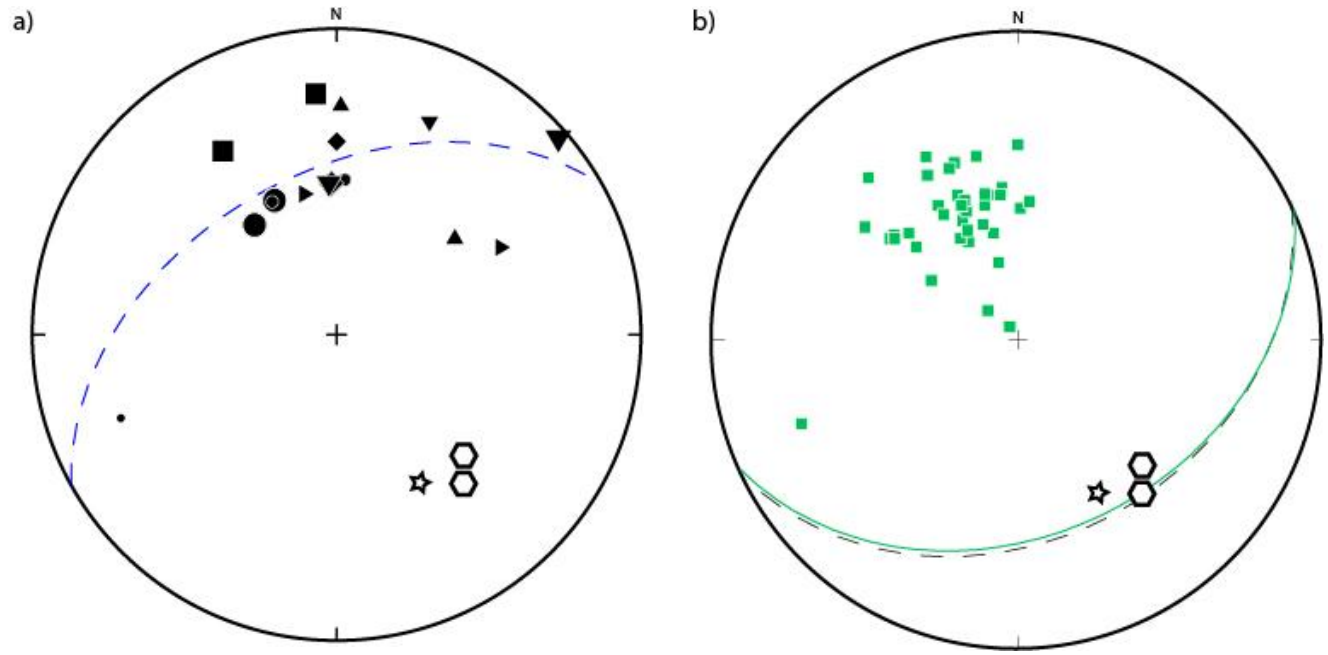

Figure 2.8: a) Stereonet of folds from folded units in section 2.1 and 2.2 showing: 1) poles to limbs of individual folds (filled shapes), 2) average profile plane of folds (blue dashed plane), 3) hinge lines of two individual folds (open hexagons), and 4) average hinge line (star). **b)** Stereonet showing: 1) NTLMZ foliation poles (green squares), 2) average NTLMZ mylonitic foliation plane (green plane), 3) average gneissic foliation of NTLSZ (black dashed plane), 4) average hinge line (star).

The folds found in these units are asymmetrical and are exposed at high angles to their profile planes. The lower limbs of the fold are often parallel with the axial planar foliation (Fig. 2.6.b). A hand sample from the folded gneiss unit in Fig. 2.9 shows the fold hinge plunging down the axial planar foliation indicating it is a reclined fold.

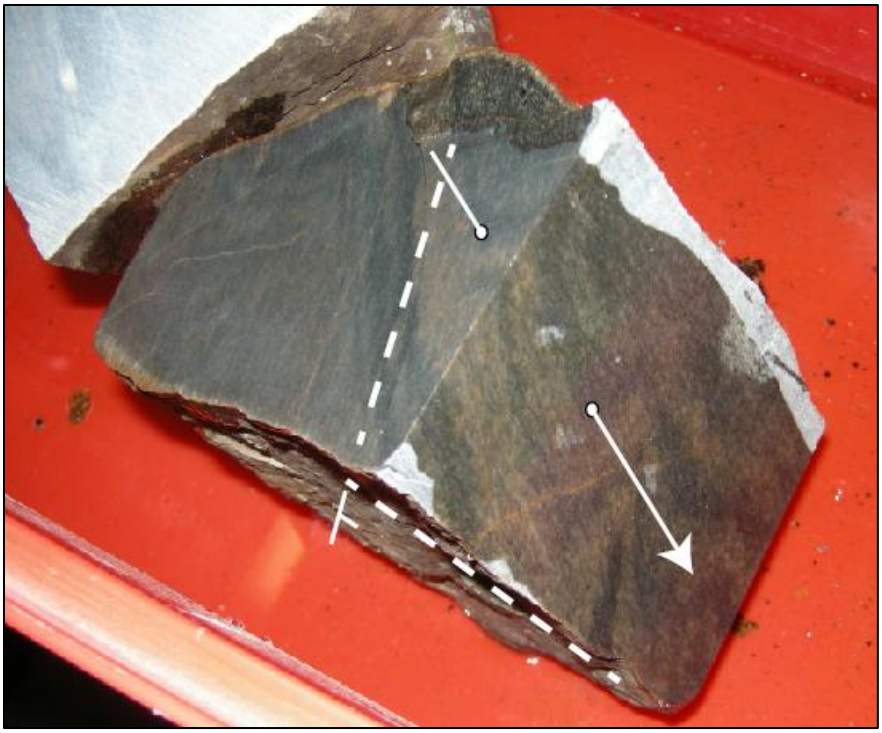

Figure 2.9: Hand sample 2.2-E showing axial planar foliation by the dashed line, and the fold hinge indicated by the solid arrow running through two locations of hinge point on the same fold. The fold hinge is plunging down dip of the foliation indicating a reclined fold.

2.5 Discussion

2.5.1 Folds

The folded units provide useful information in determining the strain regime. The asymmetrical reclined folds probably formed in a regime with a large simple shear component because the folds are asymmetrical and (see section 2.4.3). The folds likely indicate the first stage of shearing before they are strongly mylonitized. The folds are caused by simple shear folding the pre-existing gneissic banding to form asymmetrical folds. As the shearing progresses the fold hinges can be rotated into the transport direction (Culshaw 2005). Fold hinges plunge to the southeast, the same orientation as the NTLMZ foliation dips. The down dip plunge is

compatible with a normal or thrust shear sense but is likely normal as deduced from independent evidence (see chapter 4).

2.5.2 Lineation

A peculiar aspect of the mylonite zone is the lack of a widespread lineation despite evidence for plane strain in thin section. This may in part result from the lack of outcrop exposure of foliation surfaces. Alternatively, an obvious lineation may not have formed due to the fine grain size, equigranular texture and monochromatic properties of the mylonite. Nevertheless, inspection of foliation on saw cut surfaces reveals a preferred orientation of hornblende which are either aligned or perpendicular to the extension direction (SE/NW).

2.5.3 Pure vs. Simple Shear

It is thought the shear zone was formed by simple shear because the wall rocks are undeformed during the shear event and on account of the geometry of some microscopic kinematic indicators and the nature of lattice preferred orientation patterns of mylonites (Chapter 4).

2.5.4 Relationship of the NTLMZ to the North Tea Lake Shear Zone.

The NTLMZ is found within the North Tea Lake Shear Zone and mylonitizes the amphibolite facies rocks formed by the NTLSZ. The folds of NTLMZ fold the banding formed by the NTLSZ, also the NTLMZ formed at lower grade (greenschist facies) then the NTLSZ (amphibolite facies), therefore the NTLMZ formed after the NTLSZ. The foliations of the two zones are parallel (Fig. 2.8.b), indicating a similar orientation of the strain field in the formation

of these zones. The similar orientations of foliations suggest the NTLMZ may be a reactivation of the NTLSZ which exploited the pre-existing weakness created by the foliation.

2.6 Summary

The transect of the NTLMZ reveals units subdivided based on lithological and textural-structural boundaries. The NTLMZ is a mylonitic shear zone which formed within the NTLSZ. The structural observations in the field suggest the NTLMZ is a primarily simple shear, and plane strain regime. It is possible the NTLMZ is a late reactiviation of the NTLSZ.

CHAPTER 3: PETROGRAPHY

3.1 General Statement

The mylonitization observed across the NTLSZ occurred primarily within the granitoid migmatite which is further investigated to determine the minerals present. The goal of the petrographic study is to identify deformation conditions by examining how the mineral assemblage and grain size change between the protolith migmatite and the mylonitized zone. The microstructure of the mylonitized migmatite is discussed in the next chapter (Chapter 4).

3.2 Methodology

This study employs the use of petrographic microscopes and glass covered thin sections to determine which minerals are present. Electron microprobe (EMP) analysis provided data used to determine the amount of titanium present in matrix and relict biotite to estimate changes in temperature at the time of biotite growth.

3.3 Granitoid Migmatite

The migmatite shows compositional banding of leucosomes, mesosomes, and melanosomes. Melanosomes zones are defined by dark brown biotite with a grain size range of 0.5-1mm, which is typically inter-grown with or bounding blue-green hornblende porphyroblasts (0.3-10 mm). Mesosomes typically surround the hornblende and biotite; they are composed primarily of fine grained (0.1-0.5 mm) inequigranular K-feldspar with tartan twinning, quartz with equant subgrains and plagioclase. Leucosomes are much coarser grained (0.5-1.5 mm). They contain K-feldspar with tartan twining and some myrmekitic zones, quartz with elongate subgrains, and plagioclase and some biotite (0.2-0.5 mm).

3.4 Mylonitized Migmatite

Passchier and Trouw (2005) define mylonite as a foliated and usually lineated rock that shows evidence for strong ductile deformation and normally contains fabric elements with asymmetry. Protomylonites contain 10-50 % matrix, mylonite has 50-90% matrix and ultramylonite has >90 % matrix. In this study matrix is considered to be any grains below 300 µm. The mylonitized migmatite consists of three zones; 1) mylonite bands, 2) ultra-mylonite bands and 3) mylonitized leucosomes. The proportion of each zone in the outcrop is variable due to the heterogeneity of the NTLMZ. On the outcrop scale most of the mylonitized migmatite is classified as typical mylonite bands (80 % of rock), mylonitized leucosomes account for 18 % of the outcrop, and 2% of the outcrop is ultra-mylonite. Hand samples and thin sections reveal cross cutting chlorite veins through the mylonite.

3.4.1 Mylonite Bands

The mylonitized non-leucocratic bands are the dominant fabric of the NTLMZ. By a visual estimate the matrix content ranges from 40 – 70 % in these bands. Fig. 3.1 shows mylonite band with ~50 % matrix. The grain size of the matrix contains grains as small as 1 µm, and has an average grain size of 10 µm, newly formed biotite grains have an average size of 10-50 µm. Porphyroclasts within this band are grain size reduced rounded K-feldspar (0.1-0.5 mm). The matrix is composed of very fine grained biotite (Ti: 0.351 apfu) and quartz ribbons wrapped around the feldspar porphyroclasts. Hornblende porphyroclasts (0.5-1.5 mm) are present in varying abundance dependant on the particular band.

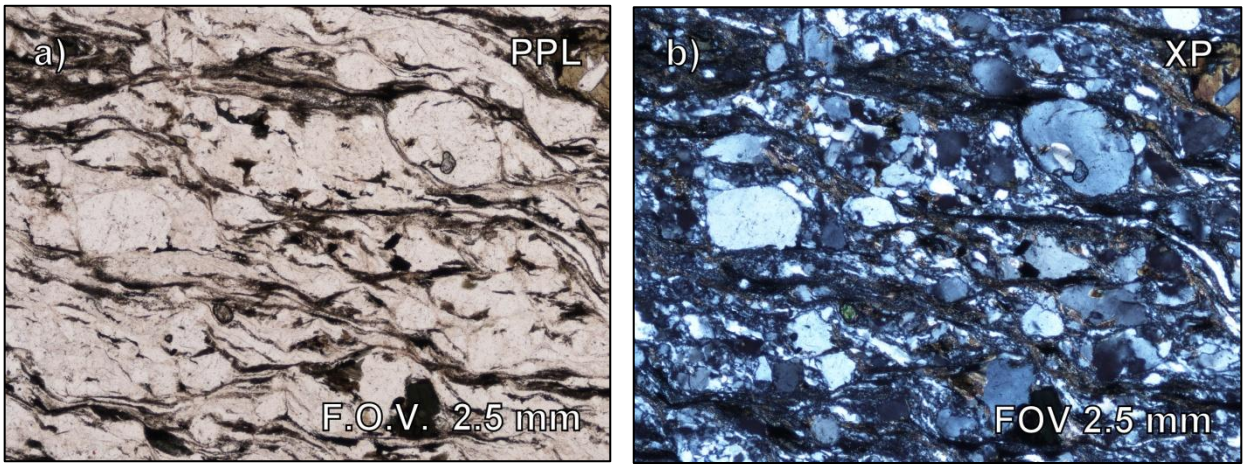

Fig. 3.1: Sample 3.3 D: Typical mylonite band with ~50% matrix showing feldspar and hornblende porphyroclasts as well as **a)** very fine dark brown matrix and **b)** coarser quartz and feldspar matrix.

3.4.2 Ultramylonite

The ultramylonite band in sample 3.3 D contains ~85-90 % matrix. The ultramylonite has large amounts of very fine grained matrix (Fig 3.2). Rounded porphyroclasts of hornblende (0.5-1 mm) and feldspar (0.1-0.25 mm) with magnetite tails (Fig. 3.2) are surrounded by a fine grained matrix of primarily biotite (average Ti: 0.394 pfu) and K-feldspar, with some hornblende and plagioclase, and traces of titanite, magnetite, and apatite.

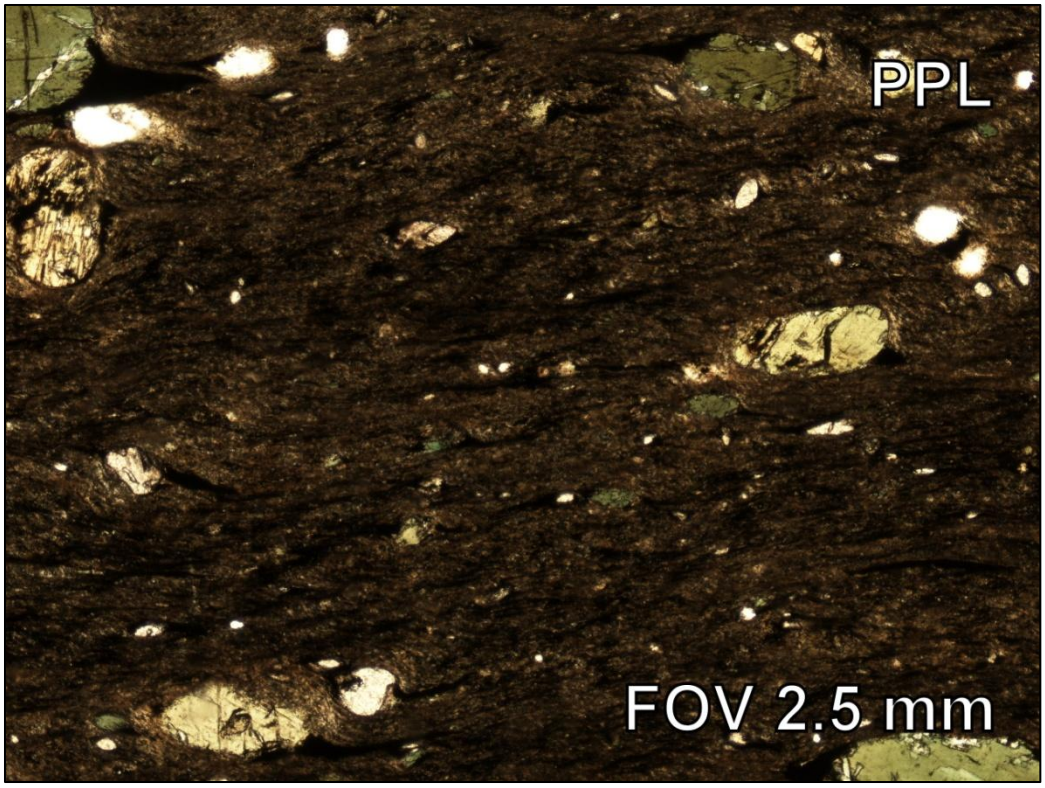

Figure 3.2: Ultramylonite zone in sample 3.3 D and bulk rock sample ARI: showing hornblende and K-feldspar porphyroclasts with magnetite tails, and very fine grained brown matrix.

3.4.3 Mylonitized Leucosomes

The mylonitized leucosomes (Fig. 3.3) are composed primarily of K-feldspar with perthitic texture and tartan twinning (0.5-4mm), plagioclase (~0.5 mm) and quartz (0.1-0.2 mm). The secondary minerals present include relict biotite (average Ti: 0.586 apfu) of a relatively larger grain size (0.1-0.2 mm) than in the mylonite or ultramylonite and minor quantities of calcite (0.1-0.3 mm) there are no hornblende porphyroclasts found in this zone.

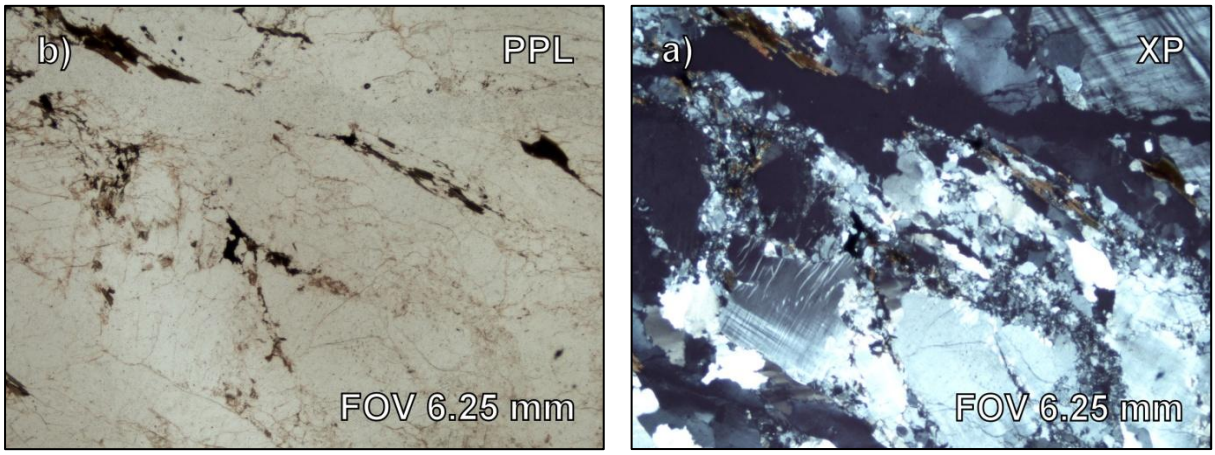

Figure 3.3: Sample 3.1 H: Mylonitized Leucosome showing a) representative felsic minerals Kfs-Qtz-Plg b) relict biotite grains within leucosome.

3.4.4 Hornblende Porphyroclasts

Hornblende porphyroclasts (Fig 3.4) are present throughout the mylonitized migmatite primarily in the non-leucocratic zones. The hornblende has many inclusions, significantly biotite grains (0.1-0.3 mm) with an average titanium content of 0.421 apfu. Fractures through the grains commonly contain chlorite. The tails of the hornblende are composed of magnetite, ilmenite, titanite and biotite.

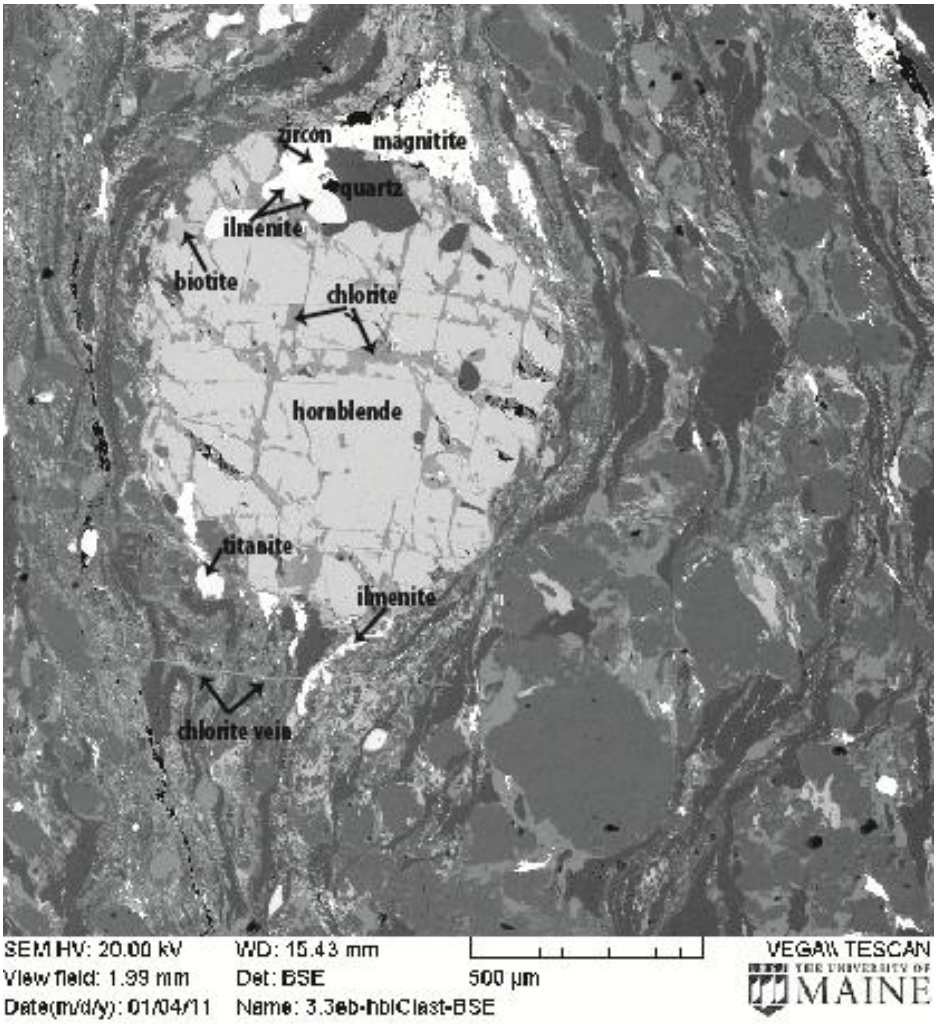

Figure 3.4: Backscatter micrograph of sample 3.3 E showing hornblende porphyroclast with inclusions of biotite, ilmenite, zircon, and late chlorite. Hornblende tails are made of magnetite, ilmenite, and fine grained biotite and K-feldspar. Also shown is a chlorite vein cross-cutting mylonite fabric.

3.5 Discussion

Greenschist conditions occur in a temperature range of 300-500 º C with a pressure of 2-8 kbar (Philpotts and Ague 2009). The mylonitization of the migmatite causes a significant grain-size reduction in the mesosomes and melanosomes and some grain size reduction in the leucosomes. The small grain size of the matrix (2-10 µm) is the main reason it is difficult to discern between deformed pre-existing minerals and minerals which grew syn-mylonitization.

The heterogeneous grain size distribution, with volumetrically dominant fine-grained fraction, indicates that grain size reduction caused by stress dominates over grain growth which occurs at hotter temperatures suggesting high stress or low to moderate temperatures during mylonitization.

3.5.1 Mineralogy

The mineral assemblage of the mylonitized migmatite does not change significantly from its amphibolite-facies protolith. Chlorite occurs in three forms 1)within hornblende fractures, 2) chloritization of biotite and 3) chlorite veins. There is not conclusive evidence to suggest chloritization of biotite or hornblende occurred during the deformation event but it is certainly possible because there is evidence of two chloritization events. The evidence of two chloritization events is that the chlorite vein is found cross-cutting a chloritized hornblende and is therefore the vein is post mylonitization and an earlier chloritization event. Epidote appears to have grown in the tail of hornblende porphyroclasts during mylonitization. If the chloritization did occur during mylonitization this would suggest green schist facies conditions.

3.5.2 Titanium Content in Biotite

Matrix biotite shows a lower titanium content (0.39 apfu in ultramylonite and 0.35 apfu in typical mylonite) compared to relict biotite (0.42 apfu in hornblende inclusions and 0.59 apfu in leucosomes) (Appendix C). Titanium content in biotite is generally lower with lower crystallisation temperatures (e.g. Henry and Guidotti 2002). Therefore mylonitization within the NTLMZ apparently occurred at lower temperatures than did migmatization or the deformation event defined within the greater NTLSZ. This also indicates that matrix biotite grew or recrystallised during mylonitization.

3.5.3 Water Content

Hydration could have occurred during retrogression of amphibolite gneiss if chloritization of biotite and hornblende occurred at mylonitization. There is no evidence of K-feldspar to muscovite reactions which would have supported a more hydrous environment.

3.5 Summary

The petrographic analysis does not indicate specific P-T conditions during deformation but does suggest low to moderate temperatures, as evidenced by the large amount of grain size reduced minerals and the potential for chloritization of minerals during deformation. The titanium content of matrix and relict biotite also indicates a lower temperature at the time of mylonitization than during protolith crystallization. The amount of hydration at the time of deformation is uncertain as K-feldspar has not retrogressed to muscovite, but biotite and hornblende may have retrogressed to chlorite in some instances.

CHAPTER 4: MICROSTRUCTURE

4.1 General Statement

The goals of the microstructural investigation are to determine the kinematics of the NTLMZ including extension direction and shear sense and to identify dynamic recrystallisation processes of each mineral. These goals are accomplished by optical microscopy of oriented thin sections and their microstructural subdomains.

4.2 Methodology

In order to determine the extension direction of the NTLMZ, which lacks an obvious lineation work was done to determine the orientation of the vorticity vector. Eleven thin sections of mylonitized migmatite cut perpendicular to the foliation were made at nine different orientations (Table 4.1). The geometry of the slides was examined to establish the sense of shear and the 'strength' of the asymmetry of sigma porphyroclasts. The orientation of the slide with the strongest asymmetry is determined to be perpendicular the vorticity vector. Because the vorticity vector is perpendicular to the extension direction the strongest asymmetry lies close to the extension direction. The shear sense is determined in the southeast dipping mylonite zone by kinematic indicators such as sigma porphyroclasts (hornblende and K-feldspar), and C' shear bands.

Deformation processes are determined through optical microscopy, by examining the dynamic microstructure of quartz, feldspar, and hornblende.

4.3 Vorticity Vector and Fabric Asymmetry

The orientation of the slides used to determine vorticity vector are shown in Table 4.1. The thin sections with the strongest asymmetric porphyroclasts are slides 3 (252º) (Fig 4.2a) and

6 (092º). The slides with no asymmetric porphyroclasts are slides 4 (160º (Fig 4.2b) and 7(002º). Slides 1(195º) and 2(100º) did not contain porphyroclasts. (Fig. 4.1)

Table 4.1 Orientation of thin section view

Slide	**1**	**2**	**3**	**4**	**5**	**6**	**7**	**8**	**9**	**10**	**11**
Sample	3.1-H	3.1-H	3.3-D	3.3-D	3.3-E	3.3-E	3.3-E	3.3-E	3.3-B	3.4-B	3.5-A
Orientation	195	100	252	160	210	92	002	210	10	290	30

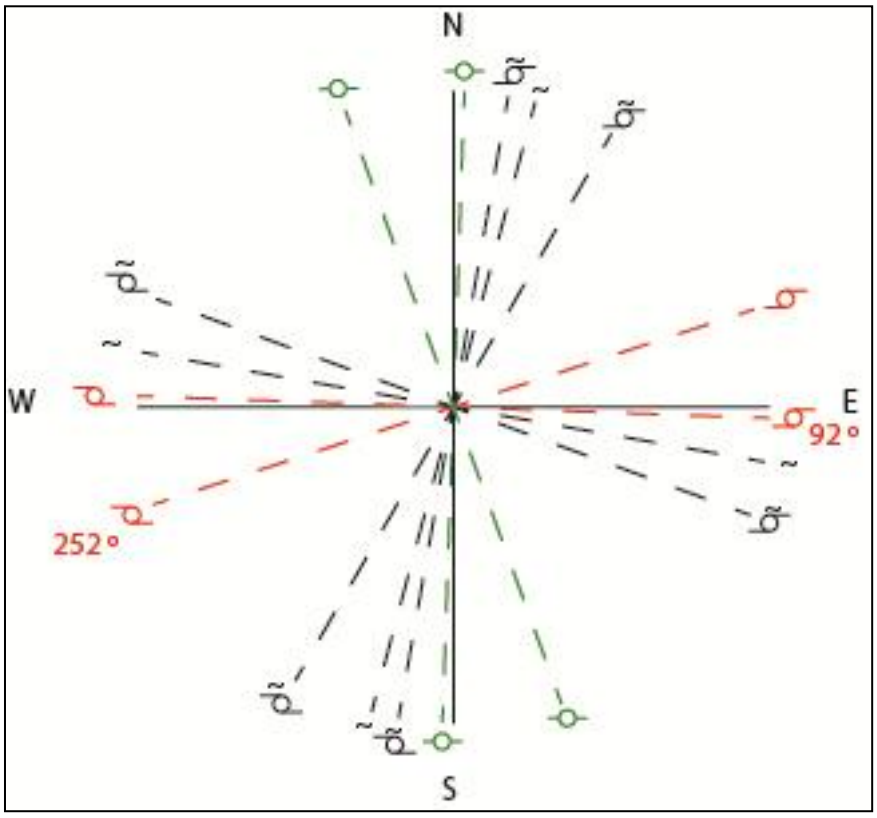

Figure 4.1: Diagram of slide orientation: line represents the viewing direction of the slide. Symbols indicate the strength of asymmetry as well as the shear sense of the porphyroclasts in each slide. Red lines show slide orientations with maximum asymmetry and therefore the lines closest to the vorticity vector, green lines show slide orientation with no asymmetry. Symbols show the shear sense of the porphyroclast in each direction. :No asymmetry, : Top to the right shear, : Top to the left shear, : Poor asymmetry, ~:No porphyroclasts.

When the viewing direction of the slide is to the southwest, the strike direction of NTLMZ foliation, porphyroclasts have maximum top to the left asymmetry (Fig 4.2.a), when slides face the southwest, parallel the strike direction of NTLMZ foliation, porphyroclasts show no asymmetry and in many cases have no tails (Fig 4.2. b). C' shear bands (Fig 4.3) and quartz grains with an SPO oblique the foliation are found in quartz ribbons (Fig 4.4.a & b).

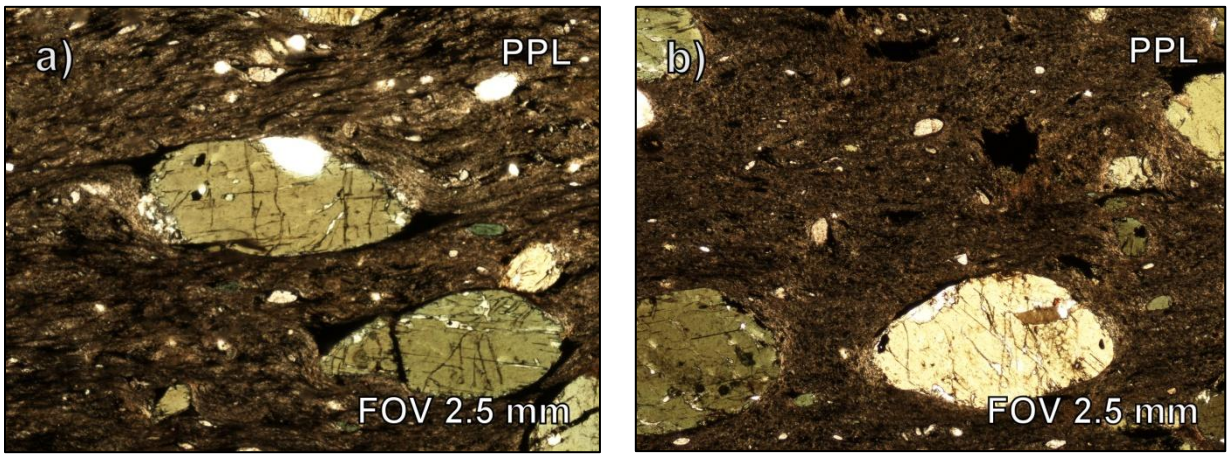

Figure 4.2: Sample 3.3 D **a)** Slide 3: Facing 252º SW showing maximum asymmetry (top to the left). **b)** Slide 4: Facing 160º SE showing minimum asymmetry.

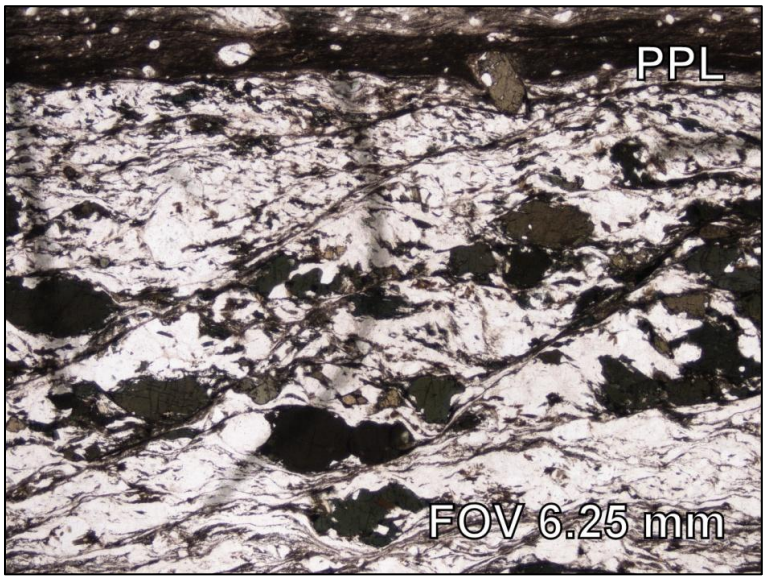

Figure 4.3: Sample 3.3 D: showing C' shear bands with top to the left shear and foliation (top dark band).

4.4 Mineral Microstructure

The quartz is found primarily in bands and feldspar porphyroclast tails. The quartz bands are very fine grained monomineralic polycrystalline with equant to moderately elongate grains. In other locations grain boundaries in aggregates of porphyroclastic quartz (0.3-0.5 mm) display interlobate texture (Fig 4.4.a).

Feldspar is found in a variety of grain sizes with angular to sub rounded boundaries as well as in the form of rounded porphyroclasts. Feldspar porphyroclasts can have a mantle of fine grained angular to sub rounded feldspar with occasional interlobate texture around the mantle (Fig 4.5.a). Some feldspars with adjacent boundaries display an interlobate textures (4.4.b). Feldspars have undulous extinction and plagioclase displays tapered deformation twins (Fig 4.4.a & 4.5 b).

Biotite grains are present as relict grains with sweeping extinction, and very fine grained blades within the matrix. Hornblende forms porphyroclasts (1-4mm) with magnetite, quartz and biotite tails. The grains are fractured and sometimes offset along the fracturing.

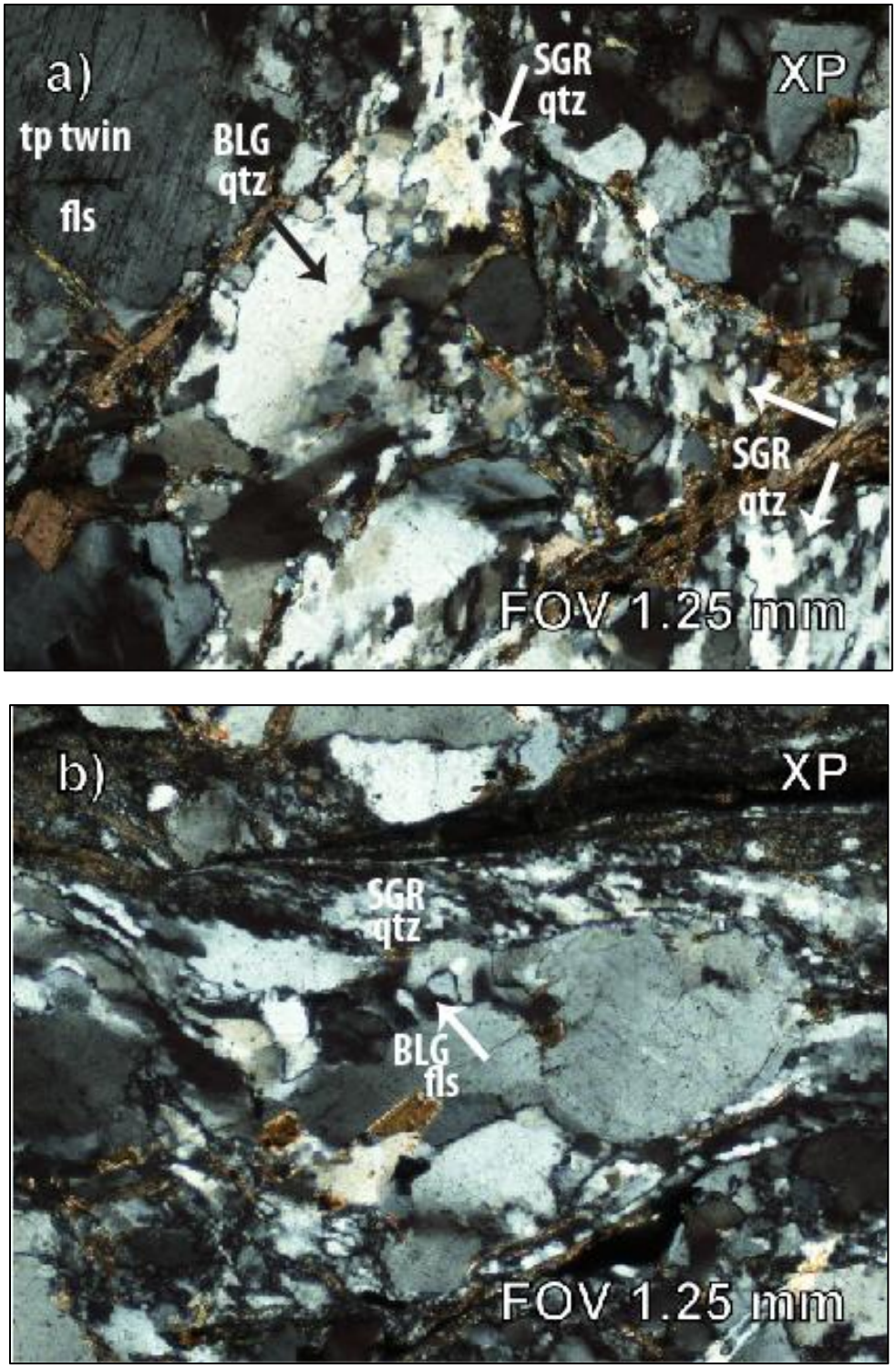

Figure 4.4: Photomicrograph **a)** Slide 6: Polycrystalline quartz bands (bottom right), interlobate quartz grain boundary of quartz porphyroclasts (middle left), angular feldspar (top right) **b)** Slide 3: Interlobate feldspar grain boundary (centre) and quartz band composed of asymmetric grains and subgrain (upper center). BLG: bulging, SGR: subgrain rotation, qtz: quartz, fls: feldspar.

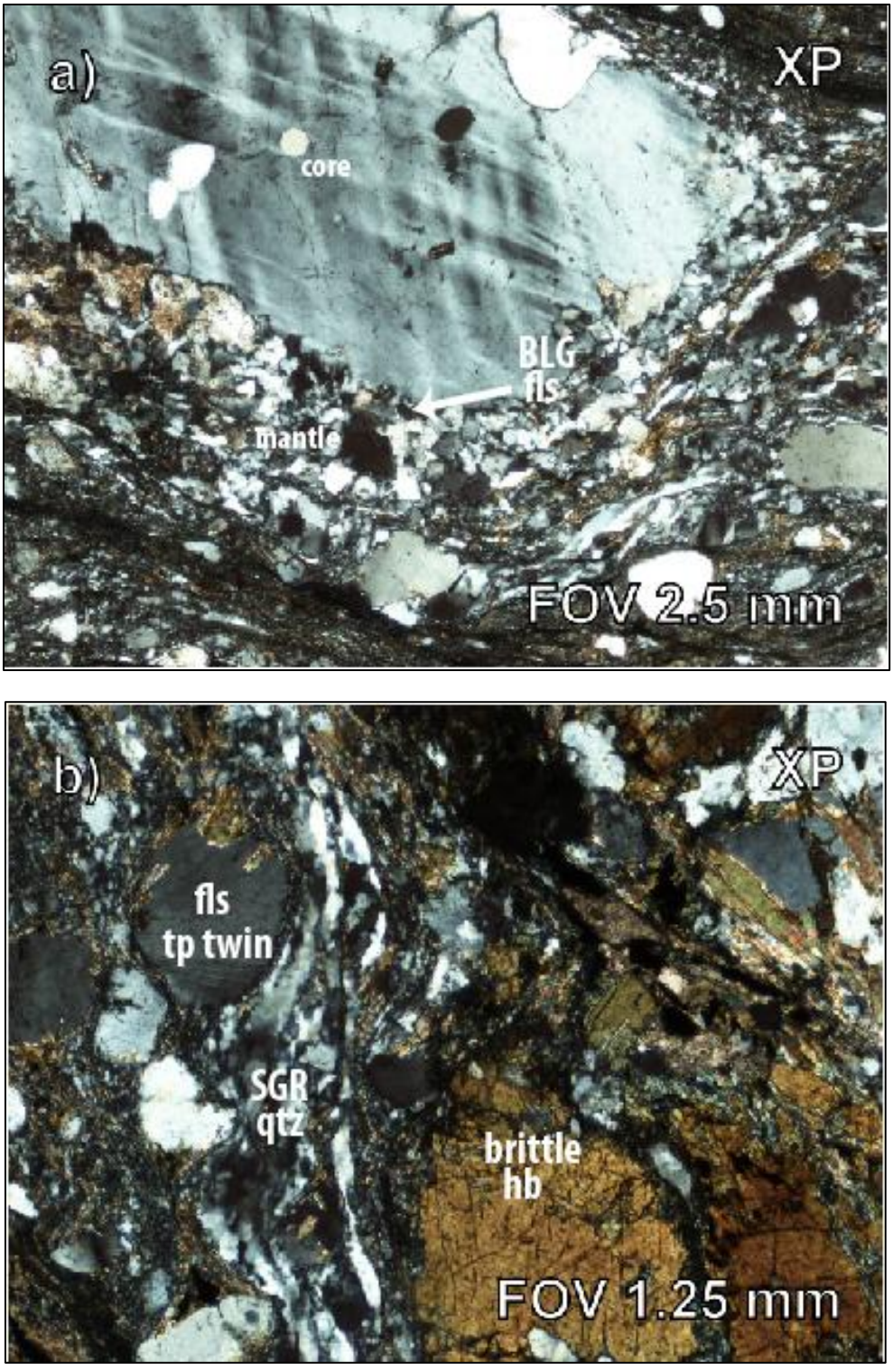

Figure 4.5: Photomicrograph: Slide 6 showing: Feldspar core and mantle texture with porphyroclast surrounded by a fine grained feldspar matrix. **b)** Slide 3 showing: plagioclase porphyroclast with tapered twins (top right), quartz band (middle) and fractured hornblende (bottom left).). BLG: bulging, SGR: subgrain rotation, qtz: quartz, fls: feldspar.

4.5 Discussion

4.5.1 Extension Direction and Shear Sense

The extension direction is interpreted to be roughly down dip the southeast dipping foliation (SSE) because the vorticity vector is apparently oriented ENE, and the vorticity vector is perpendicular the extension direction for non-coaxial flow. The shear sense is interpreted to be normal because in the southeast dipping foliation slides facing SW had top to the left shear shown by sigma-porphyroclasts and C' shear bands.

4.5.2 Deformation Processes

Each mineral in the mylonite assemblage has a unique mode of dynamic recrystallisation or brittle deformation dependant on the temperature at the time of deformation. The processes include bulging (BLG), subgrain rotation (SGR) or brittle fracture. There was no grain boundary migration (GBM) present. The deformation mechanisms are summarized in table 4.2.

Minerals with SGR are identified by equant grains in bands for example quartz bands, minerals with BLG recrystallisation are identified by presence of interlobate texture, minerals with GBM are identified by their amoeboid texture, and angular grain are indicative of brittle deformation (Passchier and Trouw 2005).

Table 4.2: Modes of Dynamic Recrystallisation or Brittle Deformation in Minerals

Mineral	Brittle	Bulging	Subgrain Rotation	Grain Boundary Migration
Quartz		X	X	
Feldspar	X	X		
Hornblende	X			

Quartz recrystallisation processes indicate a temperature of 400-500 ºC because the dominant recrystallisation mechanism is subgrain rotation which occurs most commonly in the quartz bands (Passchier and Trouw 2005).

The angular to sub-rounded texture of feldspar suggests brittle fracture. Undulous extinction can reflect internal microfracturing or dislocation glide. The rounded feldspar porphyroclasts with core mantle texture typically are formed at conditions where BLG is the dominant recrystallisation mechanism. Although interlobate texture (indicating BLG) is present, it is rare, and the angular clasts of feldspar in the mantle and elsewhere suggest brittle fracture. This suggests that a component of brittle and BLG deformation in the feldspar. The dominant process is debatable because while most of the feldspar grains are angular, core-mantle textures are thought to form by BLG. The evidence of angular grains in the mantle plus an interlobate core boundary suggests both mechanisms were active.

Brittle deformation of feldspars occurs up to temperatures of 400 º C, and at temperatures of 400-500 º C, although internal microfracturing is still the dominant deformation mechanism BLG can also occur (Passchier and Trouw 2005). Core and mantle texture do not form until medium grade temperatures of 450-600 º C when BLG is dominant (Passchier and Trouw 2005). Given these parameters the feldspar probably deformed at a temperature where brittle fracturing and BLG deformation were active such as the upper temperature range of the dominantly microfracturing with some BLG recrystallisation range (450-500 º C).

Biotite deforms ductilely, at temperatures greater than 250 ºC, whereas hornblende deforms brittlely below temperatures of 650-700 ºC. Given the temperature constraints of the

mineral deformation processes, the mylonitization event probably occurred between 400-500 ºC (Passchier and Trouw 2005).

4.6 Summary

Investigation of oriented slides suggests the NTLMZ is a normal-sense shear zone which had a transport direction very close to down dip of the NTLMZ foliation. The varying deformation processes observed in each mineral establish a deformation temperature for the NTLMZ ~ 400-500 ºC.

CHAPTER 5: EBSD ANALYSIS

5.1 EBSD General Statement

In order to determine the lattice preferred orientation (LPO) of mylonitized quartz a representative mylonite sample (3.3 E-Slide 6) was analyzed by Electron Backscatter Diffraction (EBSD) using the Scanning Electron Microscope (SEM) facilities at the University of Maine. The crystal lattice orientation of quartz was determined from automatically indexed diffraction patterns to create Orientation Imaging Micrographs (OIM) and pole diagrams.

The orientation of data plotted on a pole diagram is presented with the rock's foliation plane represented by the horizontal line (labelled TD in Fig 5.3) and lineation also lies in this plane and is represented by the east and west poles of the diagram. When the orientation of the <c> and <a> axes of quartz crystals are plotted on the pole diagram the pattern created (e.g. girdles or point maxima) can help determine the type of slip-system that was active during the quartz deformation. The symmetry of the pattern can indicate coaxial or non-coaxial strain and in asymmetric cases, the sense of shear.

In a correctly oriented thin section it is assumed the <c> axis girdle will be symmetric about the foliation. At this stage in the study it cannot be confirmed the thin section analysed (Fig 4. 1, labelled 92 º) is correctly oriented and so the data presented are preliminary results until this can be resolved.

5.2 EBSD Methodology

To collect the EBSD data, we used EDAX-TSL Digiview IV and OIM v. 5 hardware and software mounted on a Tescan Vega II Scanning Electron Microscope in the Department of Earth Sciences, University of Maine. We simultaneously collected EDS (Energy Dispersive Spectrometry) data for Mg, Al, Si, P, K, Ca, Ti, Fe elements using the EDAX Apollo40 system. Operating conditions were a working distance of 25mm, 20 kV accelerating voltage, and ~11nA beam current, with the uncoated sample tilted 70° from the beam normal. Mapping occurred on a square grid at a step size of 1 micron, with band detection minimum and maximum of 8 and 11. Orientation and Hough data were stored for post processing (Chris Gerbi, pers. comm., 2011).

The slide chosen for EBSD analysis is perpendicular the foliation and within the error of the best approximation of the extension direction (~20 º). In practice the slide may not be exactly perpendicular the foliation or be perfectly parallel the extension direction, additionally the local flow plane may be distorted and not accurately represent bulk flow. These conditions cause pole diagrams to be un-centred.

The data presented in the pole diagram required standard post processing procedures to present the data in format comparable with published data. Area 1 (Fig 5.1.a) contained a pattern symmetric about the foliation, but Area 3 (Fig 5.1.c) did not. The reason Area 3 may not have symmetric patterns is because the orientation of the slide analysed is not perfectly parallel the extension direction and the quartz deformation may reflect a heterogeneous flow field caused by the rigid porphyroclasts around it. In order to create a pole diagram that could be used to interpret mylonite conditions the data was manually rotated until the <c> axis patterns were symmetrical about the TD. At this stage in the study only the plane of rotations but not the

direction of rotations is known. The significance of these rotations on the accuracy of the data is yet to be assessed.

5.3 EBSD Results

Three areas from sample 3.3 E were selected for EBSD analysis. Each area analyzed comprises a homogeneous, polycrystalline band of dynamically recrystallised quartz grains and reflects a different micro-tectonic environment (Fig 5.1). Areas 1 and 3 were chosen for further study because they are in ribbons parallel the NTLMZ foliation but Area 2 is in a ribbon that appears to be wrapping around a porphyroclast and therefore not as representative of the NTLMZ fabric.

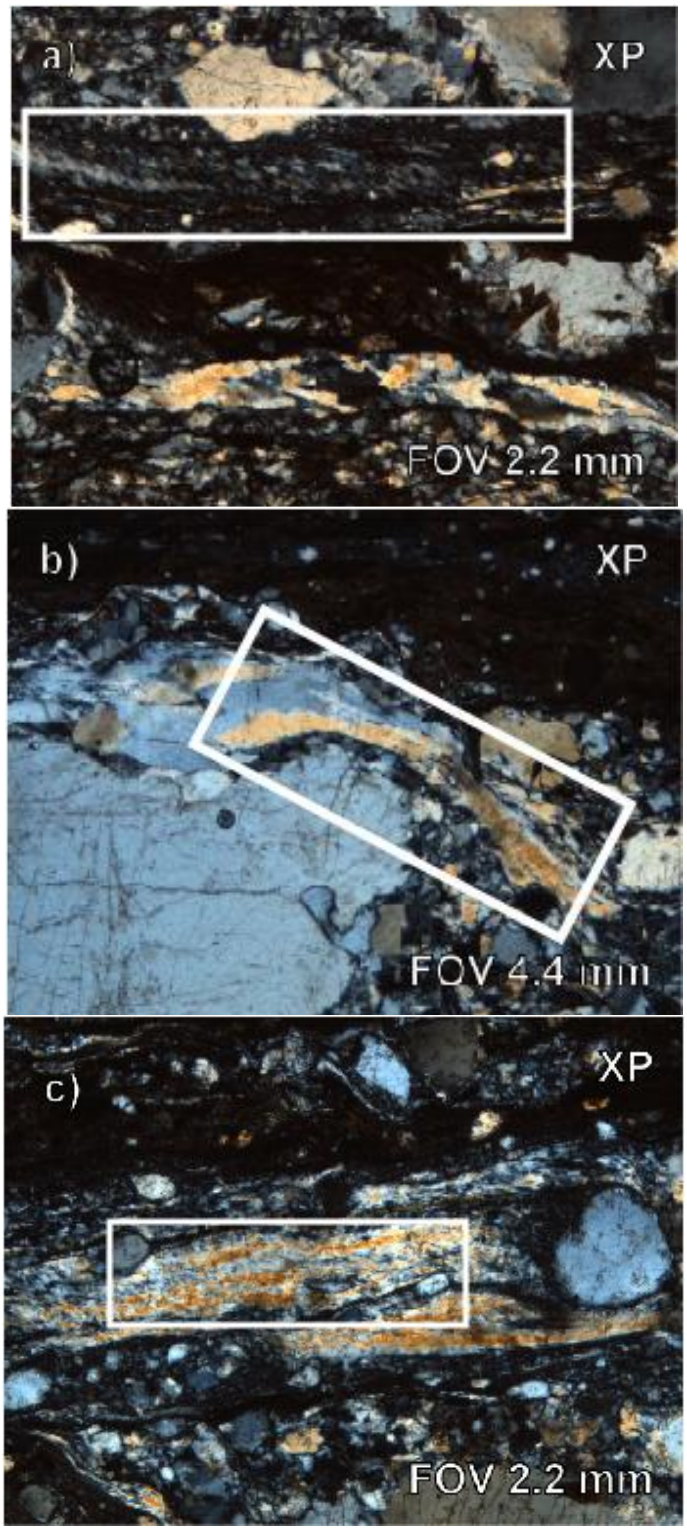

Figure 5.1: EBSD locations in Sample 3.3 E (all same slide) **a)** *Area 1* is a quartz band parallel the foliation; **b)** *Area 2* is the quartz tail of a porphyroclast and **c)** A*rea 3* is a quartz band 45 º to the foliation. (viewing direction 92 º)

5.3.1 Area 1

The analysis of Area 1 involved mapping for orientation data, but EDS data was not collected, therefore the map was cropped to an area known to contain only quartz. The quartz grains analyzed are 2-25 µm and have a shape preferred orientation (SPO) oblique to the foliation (Fig 5.2.a). Subgrains present in the area shown by the groups closely oriented equant features within a grain (Fig. 5.2.Area 1).

The pole diagram for Area 1 (Fig 5.3) has double <c> axis maxima extending from the periphery towards the centre and nearly forming a single girdle. The <a> axes show a straight girdle through the centre perpendicular the <c> axes with point maxima along the perimeters.

5.3.2 Area 3

Area 3 was mapped with EDS simultaneously with EBSD analysis to identify quartz grains and their orientation. Additional rotation of the pole figure data were required to centre the data. The rotations were 50º on TD, and 10 º on RD (The north-south line shown on pole diagram). The size of the quartz grains are 2-25 µm but have weaker SPO than Area 1 (Fig 5.2.a). Presence of subgrains is shown by the large amount of equant features with similar orientation in this area.

The pole diagram for Area 3 (Fig 4.5) has a single <c> axes girdle with strong clusters at the periphery, and a lower density through the centre of the girdle. The <a> axes pattern shows a double maxima perpendicular to the <c> axes at the periphery. There are also weaker clusters between the centre and periphery double maxima along a straight girdle.

AREA 1

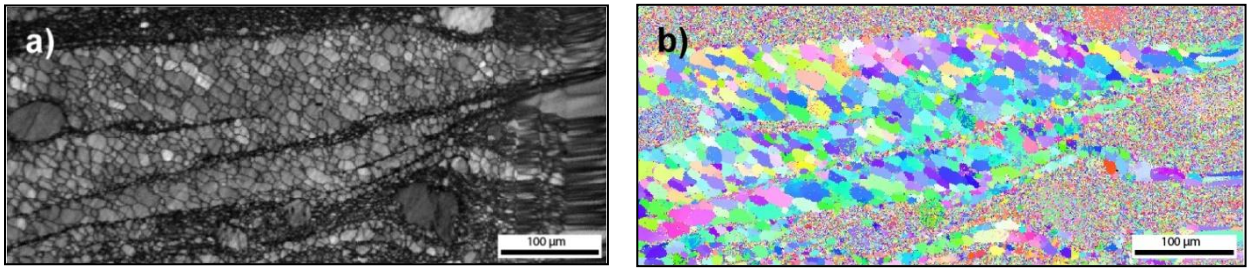

AREA 3

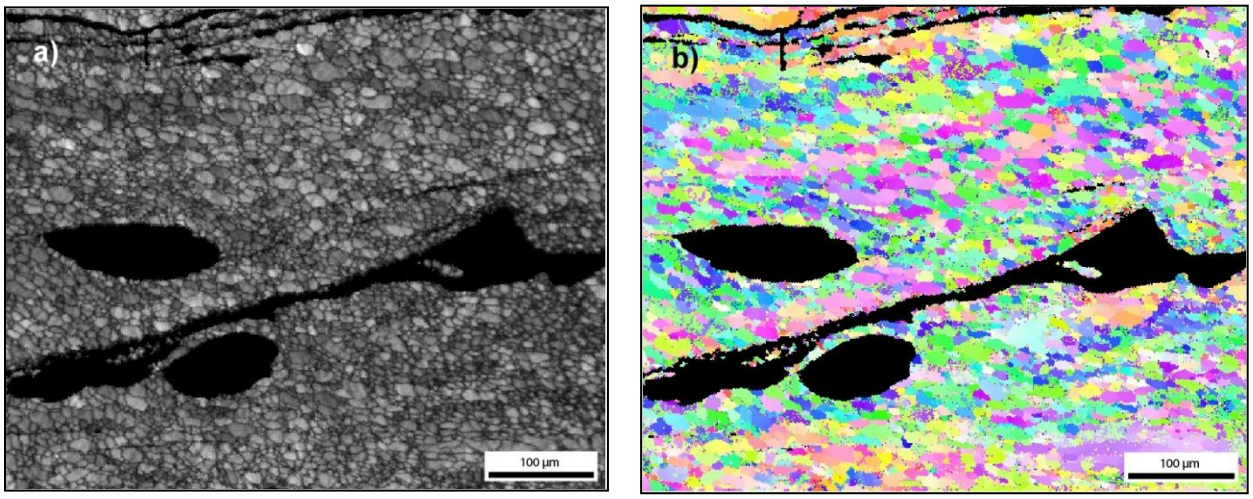

Figure 5.2: **a)** Image Quality (IQ) map showing the location of the grain boundaries and the confidence of the orientation index and **b)** Inverse Pole Figure (IPF) showing the orientation difference of grains. (See key)

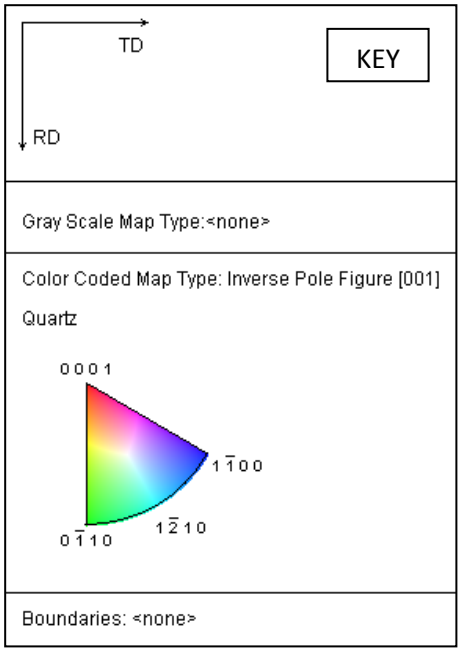

AREA 1

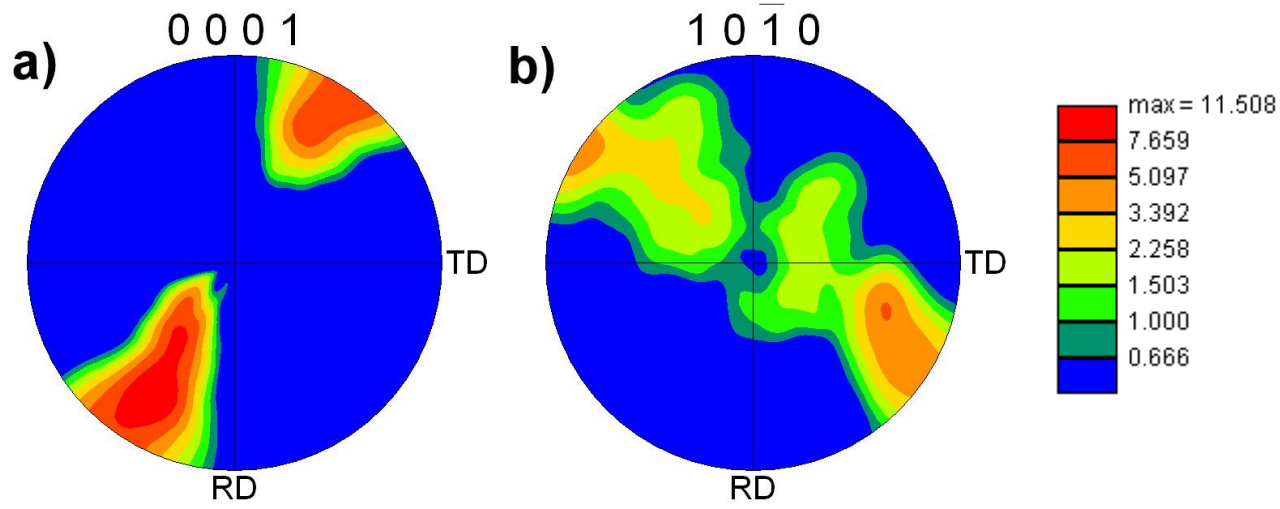

AREA 3

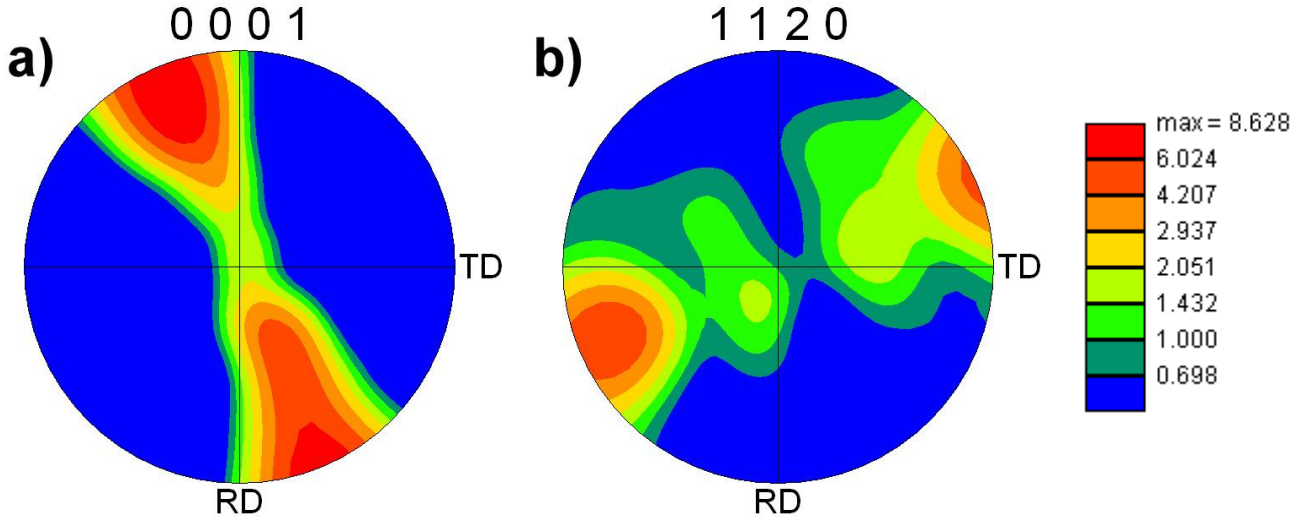

Figure 5.3: Pole diagrams of Area 1 and Area 3: **a)** <c> axes pattern and **b)** <a> axes pattern. Area 1 is facing 92 º. The orientation of Area 3 is unknown.

5.4 Grain Size

The grain size of recrystallised quartz in Area 3 was recorded during EBSD analysis, quartz ranges from 1- 70 µm. Most grains range from 8-15 µm, the mean grain size is 12 µm, which accounts for 12 % of the grains measured (Fig 5.4).

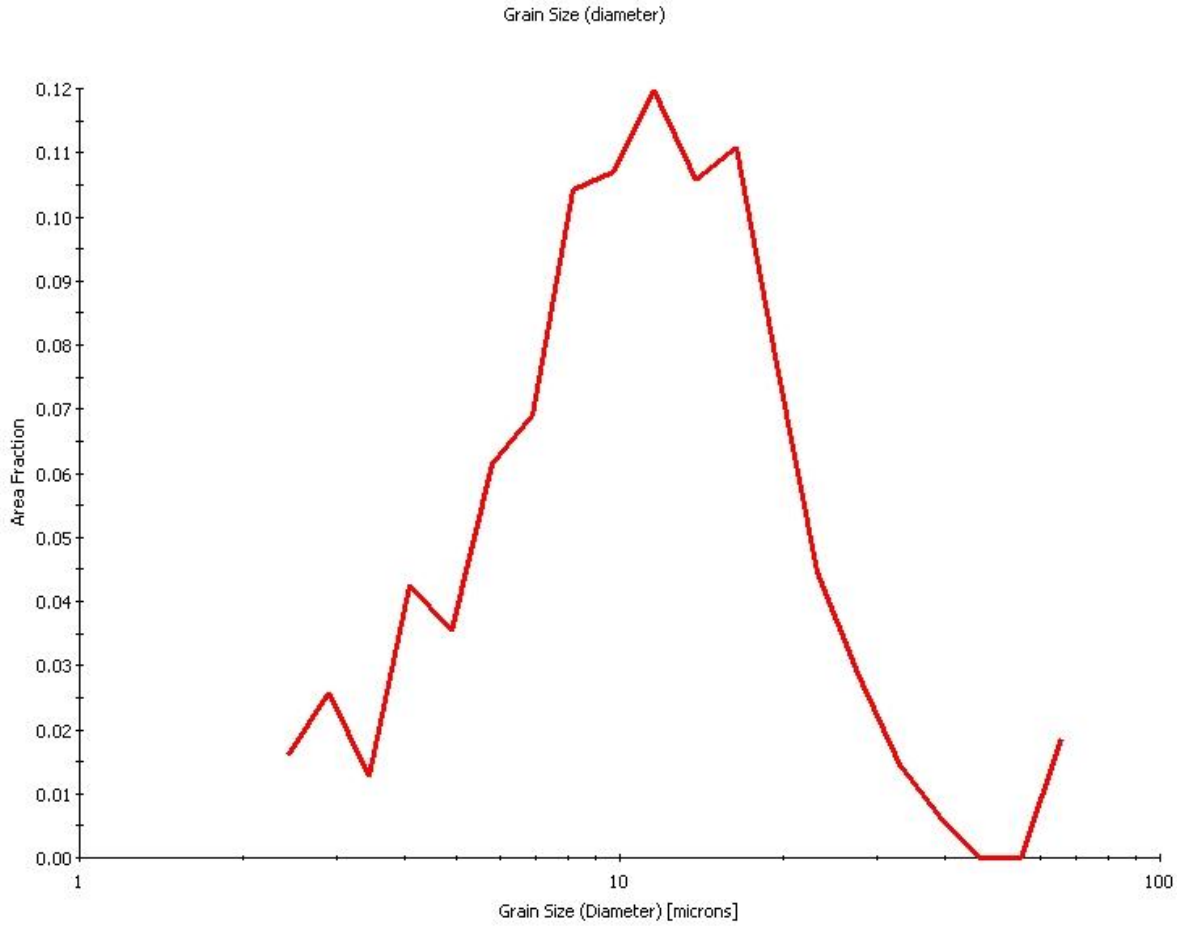

Figure 5.4: Area 3 grain size distribution of recrystallised quartz.

5.5 Discussion

5.5.1 Flow Stress

The mean recrystallised quartz grain size of Area 3 is 12 µm. This can be used as a palaeopiezometer to measure the palaeostress during mylonitization. A grain size of 12 µm correlates with a flow stress of 90 MPa (Stipp and Tullis 2003). Temperature variation does not greatly affect the palaeopiezometer in the case of quartz (Passchier and Trouw 2005). 90 MPa is relatively low in comparison to the range of stresses generally observed in the crust (up to 300 MPa) (Stipp and Tullis 2003).

5.5.2 Type of Strain

The pole diagrams in Areas 1 and 3 show <c> axes patterns with double maxima that are close to a single girdle pattern. This pattern is comparable to a plane strain pattern because it is close to a single girdle pattern (Fig 4.41: Passchier and Trouw 2005).

5.5.3 Slip Systems

The pole diagrams show double maxima <c> axes primarily in the periphery which is representative of basal <a> slip, points between the centre and edge of the pole diagram are representative of rhomb <a> slip. Prism <a> slip is represented by the points in the centre of the pole diagram which are not present in Area 1 and 3 patterns. The <a> axes are consistent with these observations (Fig 4.43: Passchier and Trouw 2005). Quartz basal <a> slip is typical of temperatures between 300-400 º C, and quartz dominated by prism <a> slip is typical of deformation temperatures between 400-500 ºC (Passchier and Trouw 2005). Rhomb<a> slip is dominant at higher temperatures than basal <a> slip and lower temperatures than prism <a> slip (Passchier and Trouw 2005). Given the presence of both basal <a> and rhomb <a> but absence

of prism <a> the temperature could be constrained to be in the upper temperature range indicated by basal <a> slip (300-400 ºC).

5.6 Summary

The EBSD data provides some useful constraints on the mylonitization event. The palaeo flow stress of quartz within the mylonite is 90 MPa as determined by the grain size distribution graph of recrystallised quartz. The pole diagram patterns suggest deformation primarily by plane strain, and the dominant slip system indicates temperatures in the upper range of 300-400 º C.

CHAPTER 6: $^{40}Ar/^{39}Ar$ GEOCHRONOLOGY

6.1 General Statement

$^{40}Ar/^{39}Ar$ geochronology study was undertaken in the Argon Lab at Dalhousie University to constrain the age of the NTLMZ. Five bulk rock samples and separates of biotite, hornblende, and a felsic concentrate were analyzed. Unfortunately the gas produced by the samples during step-heating escaped during analysis of both the biotite separate and bulk rock sample ARII and $^{40}Ar/^{39}Ar$ and data were not produced for these samples.

Potassium bearing minerals are chosen for $^{40}Ar/^{39}Ar$ as the decay of parent isotope ^{40}K occurs naturally to produce the daughter isotope ^{40}Ar by beta emission (McDougall and Harrison 1999). The $^{40}Ar/^{39}Ar$ dating method measures the time elapsed since the chosen potassium bearing mineral cooled below the temperature at which argon gas can diffuse out of the crystal lattice.

In order to obtain ages representative of the NTLMZ the samples selected for analysis must contain potassium-bearing minerals that grew at the time of mylonitization and have a closure temperature above the temperature of mylonitization, or that were reset during mylonitization. Additionally, mineral closure temperature must be higher than the temperature attained during younger thermal events so that the amount of $^{40}Ar/^{39}Ar$ will not have been reset. It is therefore important to know 1) which minerals in the sample contain potassium, 2) whether the minerals in the samples are new or relict grains and 3) the temperature at which the mylonitization event occurred.

This chapter will examine the sources of potassium in each sample as well as show the results of the ages produced by each sample and discuss their significance.

6.2 Methodology

6.2.1 Bulk Rock Samples

Bulk rock samples (AR I – V) were selected based on observations of hand samples in an effort to identify different bands of the mylonite which could reveal variation in bulk rock results. Two thin sections that contain bands representative of the bulk rock samples were used to determine detailed information on the texture and minerals of the samples. Electron Microprobe (EMP) analysis was employed to acquire a chemical map indicating the K-bearing minerals which allowed textural and grain size observations on the micron scale.

6.2.2 Mineral Separates

The biotite, felsic concentrate, and hornblende separates are from mylonitized leucosomes in Sample 3.3 E. A portion of this rock was crushed with the jaw crusher and disc mill and sieved to grain sizes between 125 – 210 µm and 210 – 500 µm. The crushed samples were then separated with a Frantz magnetic separator to create mafic and felsic concentrated separates. Biotite and hornblende were handpicked primarily from the mafic magnetic fraction of (between 0.05 – 0.2 amps). with a grain size 210 – 500 µm. The felsic magnetic separate of >0.6 amps with a grain size of 125 – 210 µm was used as the felsic concentrate.

EMP work enabled determination of the sources of K (K-bearing minerals) within the leucosome using a composition map, and hornblende Ca-K ratio from quantitative spot analyses.

6.2.3 $^{40}Ar/^{39}Ar$ Data Collection Methodology

McDougall and Harrison (1988) described the principles and method of $^{40}Ar/^{39}Ar$ dating. The separated mica concentrates were individually wrapped in aluminum foil, then stacked in an

aluminum irradiation canister. Interspersed among the samples were five to seven aliquots of the flux monitor, Fish Canyon tuff sanidine, which has an apparent K-Ar age of 28.205 ± 0.046 Ma (Kuiper et al. 2008). The canister was irradiated with fast neutrons in the nuclear reactor at McMaster University in Hamilton, Ontario, Canada. At Dalhousie University, a double -vacuum tantalum resistance furnace was used to carry out the step-heating. Isotopic analyses were made in a VG3600 mass spectrometer using both Faraday and electron multiplier collectors to measure the abundance of ^{39}Ar for $^{40}Ar/^{39}Ar$ and $^{36}Ar/^{39}Ar$ ratios, respectively. Errors are reported at the 2σ level and include the uncertainty in the irradiation parameter, J, but do not incorporate uncertainty in the assumed age of the flux monitor (Taylor, pers. comm. 2011).

6.3 Sample Descriptions

The samples selected for $^{40}Ar/^{39}Ar$ Geochronology include five bulk rock samples, a biotite separate, hornblende separate and felsic separate. Following EMP work it is observed samples AR II-V are all of the same texture and composition and so will be described together.

6.3.1Bulk Rock Sample –AR I Ultramylonite

AR I is from sample 3.3 D. The minerals containing potassium in this sample include very fine grained matrix K-feldspar and biotite, and porphyroclasts of hornblende (Fig 6.1).

6.3.2 Bulk Rock Samples AR II-V Mylonite

Argon samples AR II and AR III are from sample 3.3 D, and argon samples AR IV and AR V are from sample 3.3 E. Although some variation occurs between the bands representative of these samples in the percent matrix variation is minimal.

The occurrences of potassium in these mylonite bands are found in matrix and relict orthoclase and biotite, and hornblende porphyroclasts (Fig 6.2).

6.3.3 Felsic Concentrate and Biotite Separate

Both these samples are separated from mylonitized leucosomes. The potassium in this zone is located in the K-feldspar and biotite (Fig. 6.3.a). The potassium map in (Fig 6.4.b) confirms the only sources of potassium from this zone are K-feldspar and biotite. Visual observations of the grains show that no biotite is found in the felsic separate, and that small amounts of hornblende are found in the biotite separate.

6.3.4 Hornblende Separate

Hornblendes were separated from the same crushed sample as the biotite and felsic concentrate. The hornblende porphyroclasts are not found in leucosomes therefore the they must be from a grains adjacent to the leucosomes were also crushed and that is the source for this sample.

Hornblende EMP analysis revealed consistent composition throughout the several grains in all locations (Appendix B). It is noted the hornblende porphyroclasts contain biotite inclusions which will be accounted for by determining the calcium-potassium ratio with EMP data.

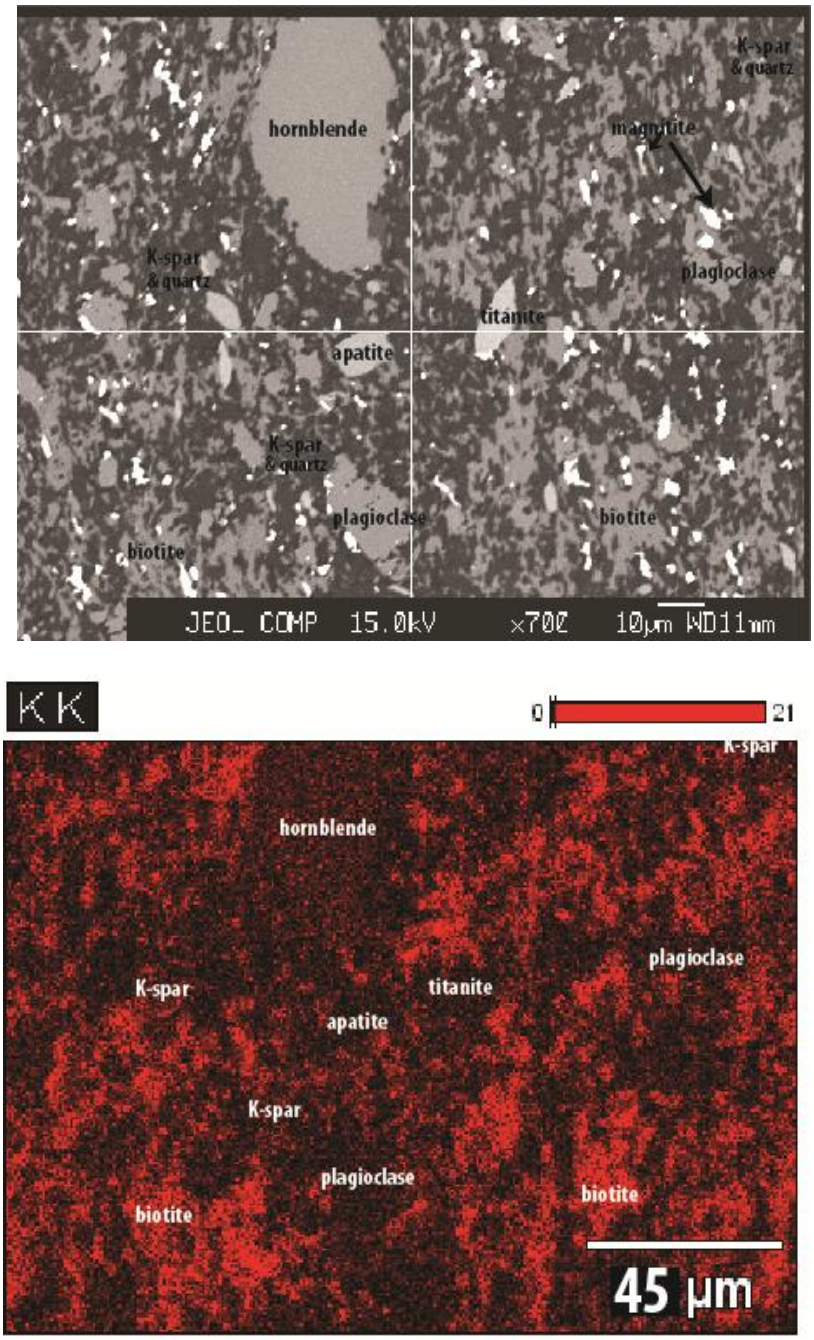

Figure 6.1: Sample 3.3 D: ARI **a)** Electron Backscatter image showing mineralogy of very fine grained ultramylonite matrix (grain size 1-15 µm) **b)** Compositional map showing minerals containing potassium: biotite, hornblende, and K-feldspar (sodium rich).

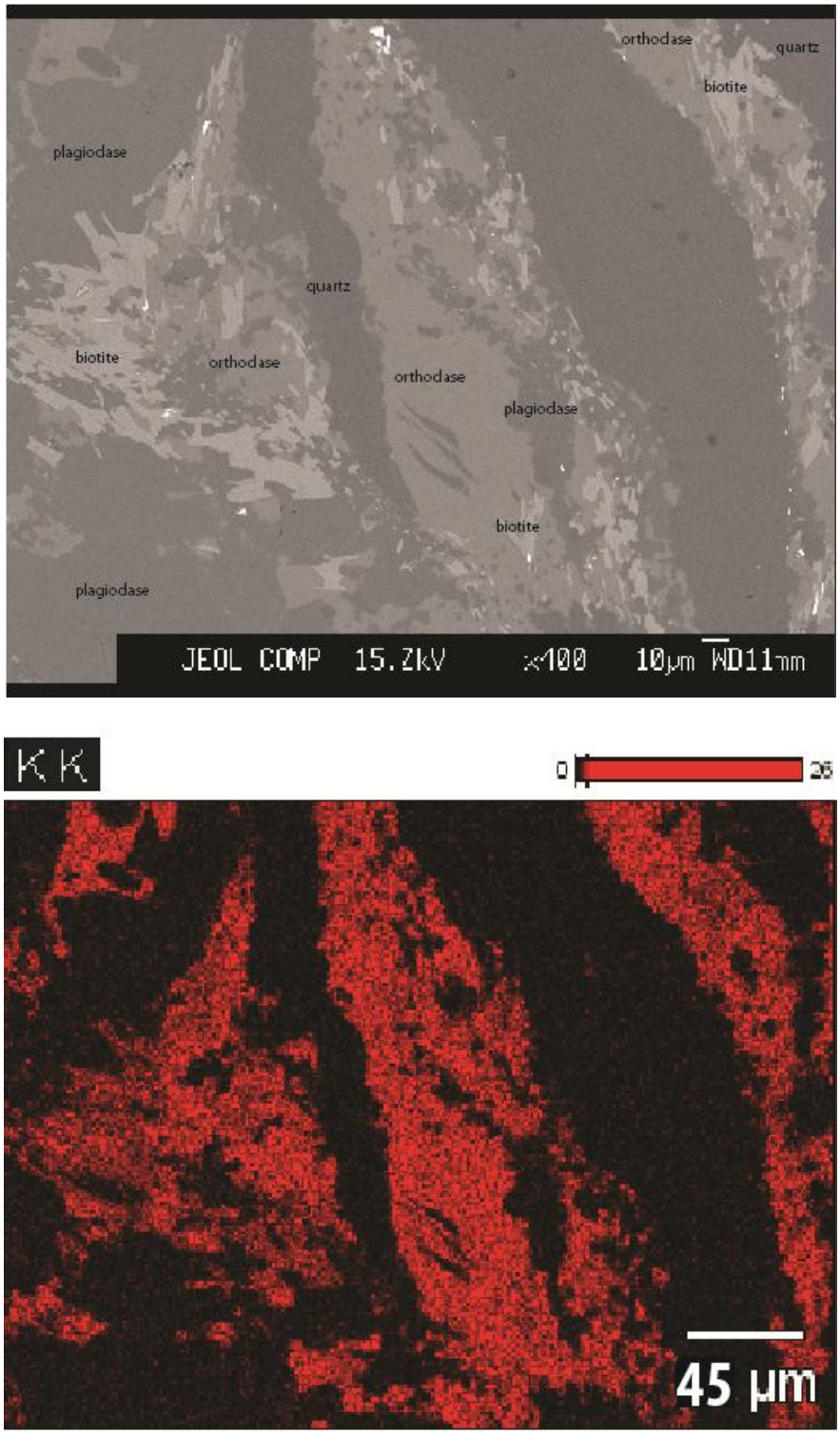

Figure 6.2: Sample 3.3 D: ARIII **a)** Electron Backscatter image showing mineralogy of fine grained mylonite matrix and tail of plagioclase porphyroclast, **b)** Compositional Map showing minerals containing potassium are biotite, hornblende (not shown), and orthoclase.

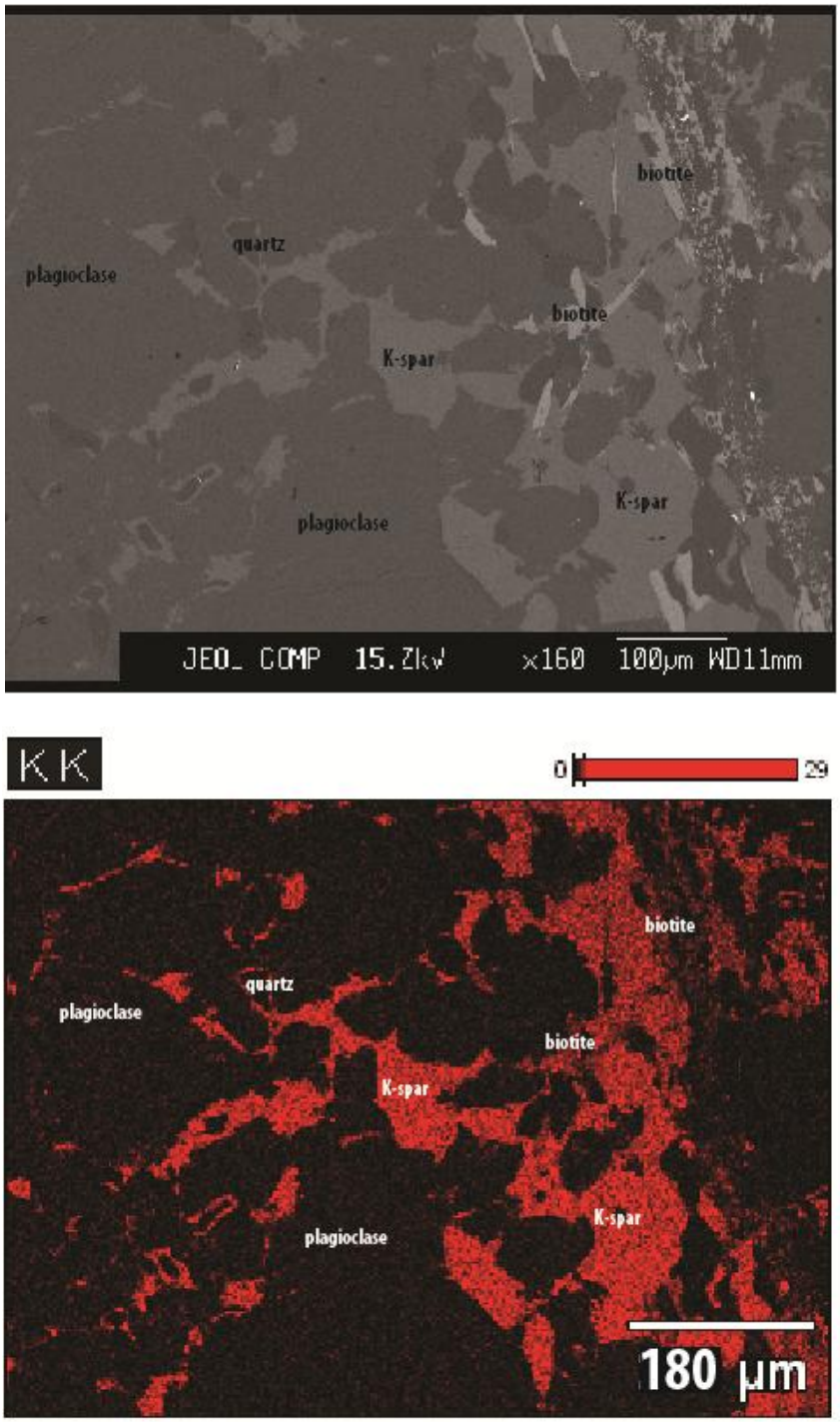

Figure 6.3: Sample 3.3 E: Source of felsic and biotite separate for ^{39}Ar/^{40}Ar dating **a)** Electron Backscatter image showing mineralogy of mylonitized leucosomes **b)** Compositional map showing minerals containing potassium: K-feldspar and biotite.

6.4 $^{40}Ar/^{39}Ar$ Data

The results of the Argon study are shown in Fig 6.4. This graph shows the measured gas of each of the six samples for which results were obtained. Individual graphs for each sample can be found in Appendix D.

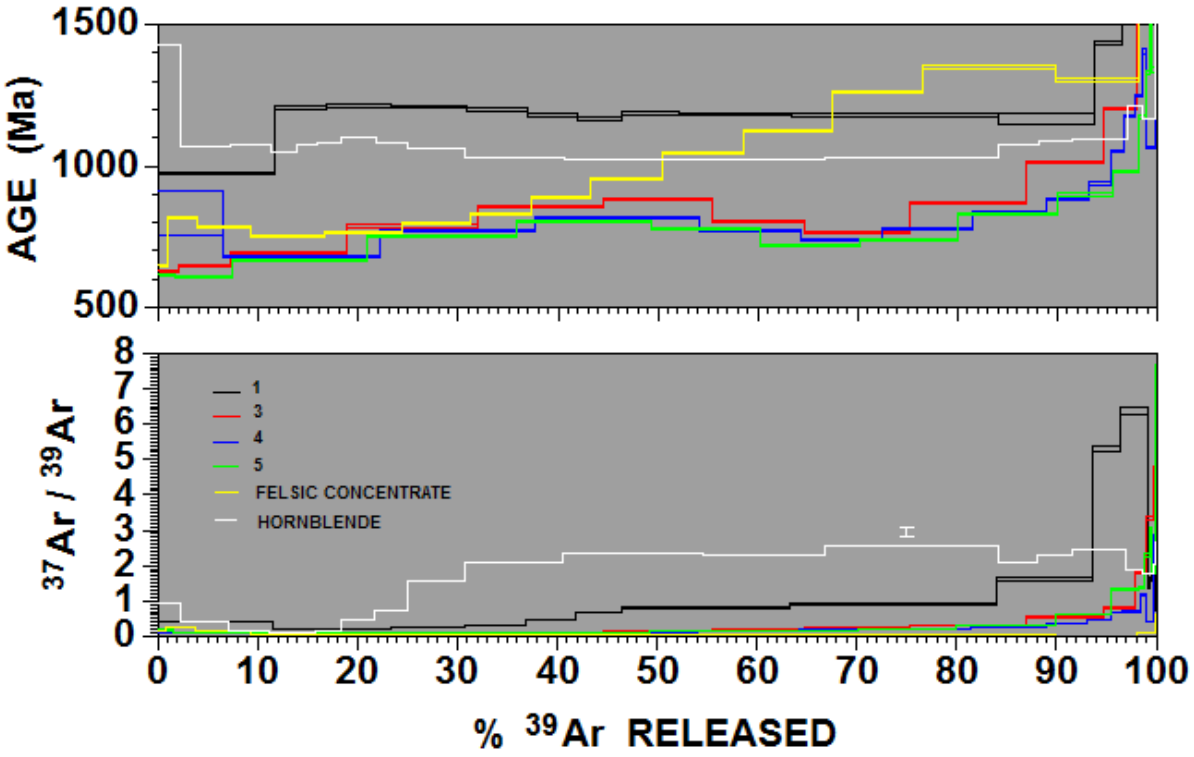

Figure 6.4: Graph showing $^{40}Ar/^{39}Ar$ data from samples processed. Note white bar representing measured Ca/K in hornblende from EMP analysis. See key in lower graph for sample ID. (Black=bulk rock sample AR I ultramylonite, red=bulk rock sample AR III mylonite, blue=bulk rock sample AR IV mylonite, green=bulk rock sample AR V mylonite, yellow=felsic concentrate separate, white=hornblende separate).

6.4.1Bulk Rock Sample AR I Ultramylonite

Sample AR I shows a plateau at 1200 Ma. The $^{37}Ar/^{39}Ar$ ratio indicates hornblende gas contributed to this age during higher temperatures of the step-wise heating process. The last 10% of gas released is dominantly hornblende gas.

6.4.2 Bulk Rock Samples AR III – V Mylonite

The data for samples AR III-V follow the same trends. There are no plateaus in the data; $^{37}Ar/^{39}Ar$ data shows a small amount of the gas released came from hornblende. The trend of the data shows an age varying between 600 and 900 Ma until remnant gas at the end of step-heating produces much higher ages.

6.4.3 Felsic Concentrate Separate

The felsic separate data also did not produce a plateau but the trend in the data is more regular. The felsic separate begins at an age around 750 Ma the progressively reaches older ages up to1400 Ma

6.4.4 Hornblende Separate

The hornblende separate produces the most regular plateau at 1025 Ma ± 19 (Fig 6.5). This plateau occurs at the same stage as the majority of the hornblende gas is released. Fig 6.4 shows the Ca-K ratio of the EMP data is very close to that of gas produced from hornblende therefore the age is representative of a hornblende separate with little contamination.

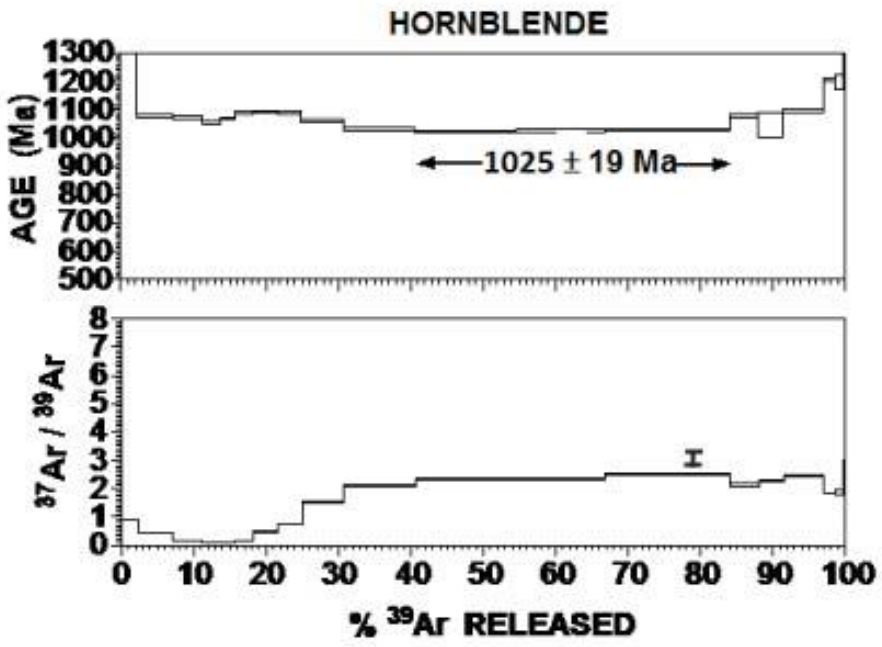

Figure 6.5: Graph showing hornblende gas released during step-heating, revealing an age of 1025 Ma with an error of 19 Ma.

6.5 Discussion

6.5.1Bulk Rock Sample AR I Ultramylonite

Although sample AR I produced a plateau with an age of 1200 Ma, the pattern produced is typical of excess argon or recoil. Due to this trend the data cannot be used.

6.4.3 Bulk Rock Samples AR III – V Mylonite

The trend displayed in all of these samples is interpreted to be an age that is the average of all the minerals present (biotite, K-feldspar and hornblende) and therefore the age presented is not a representative age of any mineral and cannot be used.

6.5.3 Hornblende Separate

The plateau presented in the hornblende data (Fig 6.5) is a good representation of the age at which hornblende closed to the diffusion of potassium and argon. The exact closure temperature for hornblende in this system is unknown but is typically close to a temperature of 490 ºC (Faure and Mensing 2005). The mylonitization event is thought to occur at temperatures lower then this (~450-500 ºC) from microstructure analysis and therefore the 1025 ± 19 Ma age of the hornblende is representative of a time in the areas cooling history prior to mylonitization of the NTLMZ.

6.5.4 Feldspar Separate

The feldspar separate data do not show a plateau providing an age. The separate does have the advantage however that it is representing only K-feldspar which has a closure temperature of 230 º C (Faure and Mensing 2005). The trend of the data starts at 750 Ma and steadily rises to ages of 1400 Ma.

Although the trend does not represent a specific time in cooling history it may be representative the polycyclic history of the area, with later thermal events resetting older ages of K-feldspar. The latest known event in the area is the intrusion of the Grenville dyke swarm at 586 Ma (Kamo et al. 1995). A Grenville dyke is located on the southern shore of North Tea Lake, and its close proximity could have partially reset the K-feldspar age.

Chapter 6: $^{40}Ar/^{39}Ar$ Geochronology

6.6 Summary

The $^{40}Ar/^{39}Ar$ study did not provide an age for the NTLMZ although ages from the hornblende and feldspar separates are representative of the areas cooling history (McLeish 2008). The hornblende analysis specifically represents a cooling age of 1025 ± 25 Ma when the study area was at ~500 º C.

CHAPTER 7: DISCUSSION

7.1 General Statement

This study presents structural, lithological, temperature, and geochronological findings for the NTLMZ. Although the kinematics of the NTLMZ are well constrained the temperature and age of the shear zone are left open to some interpretation. In this chapter a model to determine the age of the NTLMZ is discussed as well as the context of the NTLMZ to the history of the Grenville orogeny.

7.2 Age Model

The temperature of formation of the NTLMZ is still up for some debate. Titanium content of relict and new biotite indicate mylonitization occurred at temperatures lower than the amphibolite facies protolith (McLeish 2008). Study of the dynamic recrystallisation mechanisms of quartz and feldspar in the mylonite suggest a temperature of 400-500 º C. Study of the glide planes in quartz with EBSD techniques suggest a temperature of 300-400 º C. For the purpose of this discussion the common temperature of the two methods, 400 º C will be considered the deformation temperature of the NTLMZ.

The only reliable age produced by the ^{40}Ar / ^{39}Ar study is from the hornblende separate which gave a cooling age of 1025 ± 19 Ma at 500 º C. This hornblende age is comparable to hornblende ages obtained in the north of the Bonfield domain also at 1025 Ma (Cosca 1991).

If cooling continued at a rate typical of the Grenville until the mylonitization event the age of the NTLMZ can be determined. A typical CMB cooling rate is 2-4º C Myr $^{-1}$ (Cosca 1991) and for the purpose of this model a cooling rate of 2 º C Myr $^{-1}$ is assumed. Figure 7.1 plots these variables.

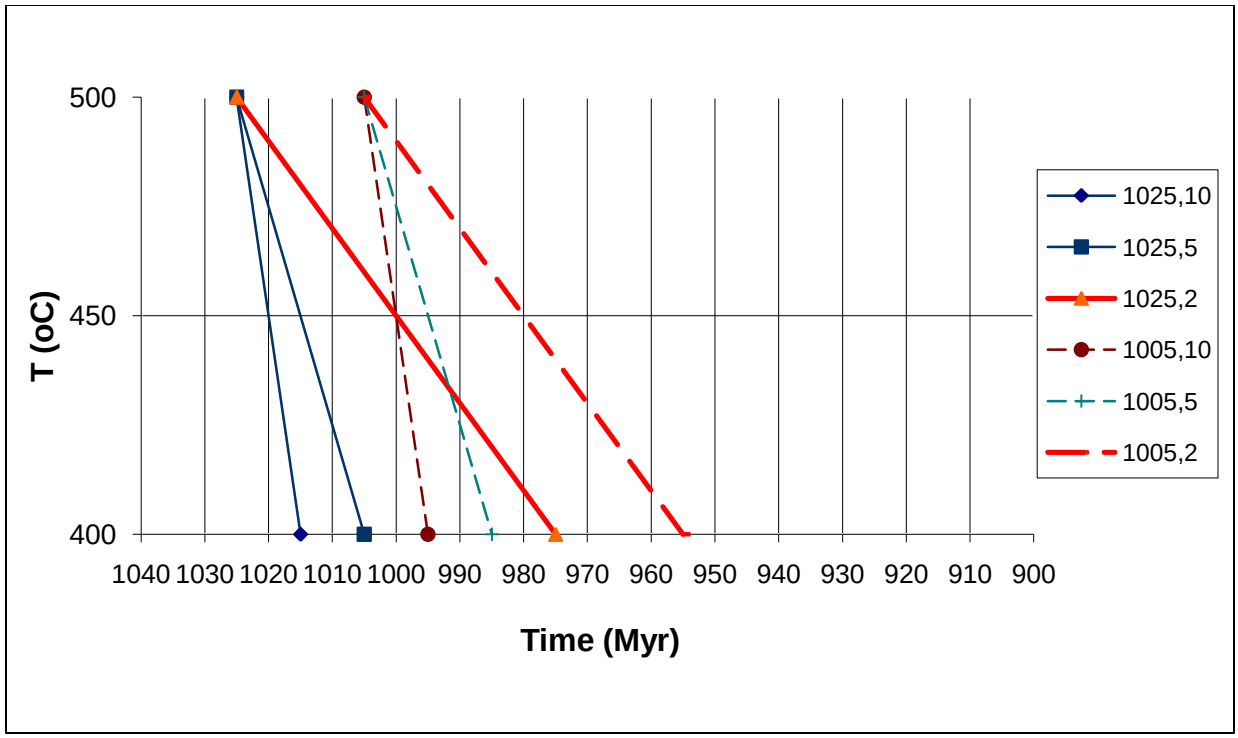

Figure 7.1: Graph showing the age of the hornblende separate (1025 Ma or 1005 Ma) at its closure temperature (500 ºC) and possible cooling rates of (10, 5 or 2 º C Myr $^{-1}$) until cooling trends reach the probable temperature of mylonitization (400 º C) at which point the age of the NLTMZ can be predicted.

If the hornblende age is 1025 Ma, with a cooling rate of 2 º C Myr $^{-1}$ the mylonitization event would have occurred at 975 Ma. With these same parameters but a hornblende age of 1005 Ma the mylonitization event would have occurred at 955 Ma.

If the cooling rate was different by 3 º C Myr $^{-1}$ the age would have changed by 10 Ma, and if the mylonitization temperature was changed by 50 º C the age of deformation would have changed by 25 Ma. The temperature of the mylonitization is the most important variable in this age model when using low cooling rates typical of Grenville cooling.

7.3 Late Extensional Features in the Grenville

If the NTLMZ occurred at an age of 975 – 955 Ma it is a late to post Grenvillian extensional feature of the Grenville orogeny (1190- 980 Ma). With a typical geotherm of 25 º C km $^{-1}$ and a mylonitization temperature of 400 º C the NTLMZ would have deformed at a depth of 16 km. In a 50 km thick crust the NTLMZ would have formed in the upper third of the crust. Several other late Grenville extensional mylonites have been identified in the CMB (Culshaw 1985; Cosca 1991) suggesting a late orogenic extension perhaps during uplift in the CMB of the Grenville orogeny.

CHAPTER 8: CONCLUSIONS

8.1 Conclusions

1. The North Tea Lake Mylonite Zone (NTLMZ) is found conformably within the North Tea Lake shear zone bounding the Kiosk and Bonfield domains. While the NTLSZ is thought to be a thrust zone (McLeish 2008) the NTLMZ is an extensional feature which reactivates the NTLSZ.

2. Field observations and optical study of microstructure indicate the NTLMZ is a normal-sense extensional shear zone with primarily simple shear in a plane strain regime. EBSD analysis suggests a quartz flow stress of 90 MPa in the NTLMZ.

3. The extension direction of the shear zone is down dipof the foliation, this is indicated by fold hinges which appear to have rotated parallel the dip and a best estimate of the vorticity vector to be perpendicular dip.

4. Temperature of the NTLMZ was constrained by dynamic recrystallisation mechanisms (400-500 º C), quartz slip planes (basal <a>, 300-500 º C) and the mineral assemblage (300-500 ºC) to have a preferred value of 400 º C.

4. The age of the NTLMZ can be modeled from the stepwise ^{40}Ar/ ^{39}Ar degassing of hornblende which indicates a cooling age of 1025 ± 19 Ma and with an assumed CMB cooling rate of 2 ºC Myr $^{-1}$ to have occurred between ~ 975 -955 Ma.

5. With a temperature assumption of 400 º C during mylonitization the NTLMZ deformation is expected to have occurred at a depth of 16 km between 955 – 975 Ma with an assumed geotherm of 25 º C per km. The hornblende age is representative of NTLSZ event, which formed in amphibolite facies conditions (500-750 º C). With the same geotherm assumption the NTLSZ

formed at depths 4-10 km greater than the NTLMZ indicating a period of exhumation in the study area between 1025 Ma and 975 – 955 Ma.

8.2 Recommendations for Further Study

Further investigation of the NTLSZ involves follow up on the objectives of this study with more detailed analysis. 1) A further temperature constraint could be conducted by measuring the titanium content of quartz (Wark 2006), 2) Several samples of biotite separate should be analyzed with $^{40}Ar/^{39}Ar$ techniques for a more direct determination of NTLMZ age 3) The EBSD data collected should be further investigated to ensure pole diagrams are presented perpendicular the foliation and parallel extension direction and finally 4) a detailed literature review should be carried out to relate the late extensional NTLMZ to similar features within the CMB, CGB and Grenville province to build understanding of late orogenic processes.

REFERENCES

Carr, S. D., Easton, R. N., Jamieson, R. A., and Culshaw, N. G. 2000. Geologic transect across the Grenville orogen of Ontario and New York. Canadian Journal of Earth Science, ***37:*** 193-194.

Cosca, M. A., Sutter, J. F, and Essene, E. J. 1991. Cooling and inferred uplift/erosion history of the Grenville orogen, Ontario: Constraints from ^{40}Ar/ ^{39}Ar Thermochronology. Tectonics, **10**: 959-977.

Culshaw, N. 2010. Aspects of the Geology of Algonquin Park.

Culshaw, N. G., Buckle folding and deep-crustal shearing of high-grade gneisses at the junction of two major high-strain zones, Central Gneiss Belt. Grenville Province, Ontario. Canadian Journal of Earth Sciences, **42**, 1907-1925

Culshaw, N. 1987. Microstructure, c-axis pattern, microstrain, and kinematics of some S – C mylonites in Grenville Gneiss. Journal of Structural Geology, **9**: 299-311

Culshaw, N. G., Jamieson, R. A., Kethchum, W. F., Wodicka, N., Corrigan, D. & Reynolds, P. H. (1997). Transect across the northwestern Grenville orogen, Georgian Bay, Ontario: Polystage convergence and extension in the lower orogenic crust, Tectonics, **16***:* 966-982.

Faure, G. and Mensing T. M.2005. Isotopes Principles and Applications Third Edition. John Wiley & Sons, Inc. Hoboken, New Jersey.

Henry, D. J., and Guidotti, C. V. 2002.Ti in biotite from metapelitic rocks: Temperature effects, crystallochemical controls and petrologic applications. American Mineralogist, **87**: 375-382.

Kamo, S. L., Krough, T. E, and Kumarapeli, P. S. 1995. Age of Grenville dyke swarm, Ontario-Quebec: implications for the timing of the Iapetan rifting, Canadian Journal of Earth Scineces, **32**: 273-280

Kuiper, K.F., Deino, A., Hilgen, F.J.,Krijgsman, W.,Renne, P.R. and Wijbrans, J.R. 2008.Synchronizing rock clocks of Earth history, Science, **320**: 500-504.

MacDougall, I and Harrison, T.M. 1988. Geochronology and thermochronology by the 40Ar/39Ar method. Oxford University Press, New York.

McLeish, D. F. 2008. Geology, petrology, and metamorphic history of western Algonquin Park: Implications for the evolution of the western Grenville orogen. Senior Thesis.

Passchier, C. W., and Trouw, A. J. 2005. Micro-tectonics. Springer-Verlag Berlin Heidelberg, Germany.

Philpotts , A., and Ague, J. 2009. Principles of Igneous and Metamorphic Petrology. Cambridge University Press, New York.

Stipp, M., and Tullis. 2003. The recrystallised grain size piezometer for quartz. Geophys Res Lett. **30**: 2088

Vernon, R. H. 2004. A practical guide to rock microstructure, Cambridge University Press, New York.

Wark, D. A., and Watson, B. 2006. TitaniQ: a titanium-in-quartz geothermometer. Contrib Mineral Petrol. **152**: 743-754

APPENDIX A: ABBREVIATIONS USED IN TEXT AND DIAGRAMS

^{40}Ar/^{39}Ar- Argon-40/Argon-39 (Geochronological technique)

BLG- Bulging

CMB- Central Metasedimentary Belt

EBSD- Electron backscatter diffraction

EDS- Energy Dispersive Spectrometry

EMP- Electron Microprobe

GBM- Grain Boundary Migration

GFTZ- Grenville Front Tectonic Zone

LPO- Lattice preferred orientation

NTLMZ- North Tea Lake Mylonite Zone

NTLSZ- North Tea Lake Shear Zone

SPO- Shape preferred orientation

SGR- Subgrain rotation

Appendix B

Table B.1: Amphibole analyses

Sample	33D_ARI_1	33D_hbl_1	33D_hbl_2	33D_hbl_3	33D_hbl_4	33D_hbl_5	33D_hbl_6	33D_hbl_7	33D_hbl_8	33D_hbl_9
No.	13	72	73	74	75	76	77	78	79	80
Wt.%										
SiO2	40.8802	41.3102	40.7236	40.3684	41.1165	41.313	41.2252	41.0391	41.1936	40.9642
TiO2	0.946	1.469	1.4545	0.9374	1.6999	1.7088	1.7086	1.4947	1.6983	1.4462
Al2O3	12.2459	11.7933	11.6778	12.1056	11.7555	11.6333	11.6924	11.4555	11.4534	11.722
FeO	17.9823	18.8754	19.2623	19.0707	19.0827	18.634	19.232	18.6964	18.693	19.1381
MnO	0.5116	0.801	0.8254	0.8022	0.7669	0.7558	0.7909	0.7622	0.8073	0.8024
MgO	8.7927	8.4026	8.4435	8.5989	8.6603	8.7752	8.5738	8.799	8.7038	8.6084
CaO	11.3941	11.7745	11.5198	11.6077	11.6729	11.4135	11.3002	11.5647	11.4774	11.3745
Na2O	1.704	1.6636	1.7865	1.5452	1.8297	1.9336	1.8532	1.8192	1.892	1.802
K2O	1.5016	1.7389	1.7549	1.7514	1.7463	1.6697	1.6978	1.7271	1.7517	1.8114
Cr203	0.036	0.0648	0.0692	0.0549	0.086	0.0481	0.0731	0.0648	0.049	0.0465
Total	95.9945	98.0245	97.6864	96.9965	98.6153	98.0525	98.321	97.5952	97.8857	97.8548
Cations	(calculated on the basis of 23 O)									
Si	6.3432	6.3340	6.2918	6.2715	6.2843	6.3248	6.3123	6.3251	6.3278	6.3050
Ti	0.1104	0.1694	0.1690	0.1095	0.1954	0.1967	0.1967	0.1732	0.1962	0.1674
Al	2.2395	2.1312	2.1264	2.2166	2.1176	2.0990	2.1100	2.0809	2.0736	2.1264
Fe	2.3335	2.4204	2.4889	2.4778	2.4392	2.3858	2.4627	2.4098	2.4014	2.4635
Mn	0.0672	0.1040	0.1080	0.1056	0.0993	0.0980	0.1026	0.0995	0.1050	0.1046
Mg	2.0336	1.9204	1.9445	1.9913	1.9730	2.0025	1.9568	2.0214	1.9929	1.9750
Ca	1.8943	1.9343	1.9069	1.9322	1.9115	1.8722	1.8539	1.9097	1.8890	1.8758
Na	0.5126	0.4946	0.5352	0.4654	0.5422	0.5740	0.5502	0.5436	0.5635	0.5378
K	0.2972	0.3401	0.3459	0.3471	0.3405	0.3261	0.3316	0.3396	0.3433	0.3557
Total	15.8316	15.8484	15.9165	15.9169	15.9029	15.8790	15.8768	15.9028	15.8926	15.9111

Table B.2: Amphibole analyses

Sample	33D_hbl_10	33D_hbl_11	33D_hbl_12	33D_hbl_13	33D_hbl_14	33D_hbl_15	33D_hbl_16	33D_hbl_17	33D_hbl_18
No.	81	82	83	84	85	86	87	88	89
Wt.%									
SiO2	41.4035	41.2903	41.0683	41.0913	40.8965	41.4393	40.8676	41.4768	41.2886
TiO2	1.305	1.3053	1.4207	1.4426	0.6648	1.3068	1.4033	1.0775	1.2048
Al2O3	11.669	11.6528	11.7233	11.7808	11.9807	11.8906	11.5951	11.6668	11.5708
FeO	18.8252	18.752	18.6285	18.8515	18.8365	18.9416	18.6688	18.9618	18.8034
MnO	0.77	0.7861	0.7891	0.8384	0.7913	0.7593	0.8061	0.7774	0.742
MgO	8.7264	8.7479	8.6517	8.5589	8.9348	8.7762	8.7504	8.8302	8.8201
CaO	11.5225	11.6332	11.5257	11.5988	11.8127	11.5769	11.4928	11.5657	11.5217
Na2O	1.8114	1.7687	1.7953	1.8217	1.5317	1.7996	1.8276	1.8233	1.8685
K2O	1.7457	1.6919	1.6708	1.7014	1.6623	1.7067	1.7511	1.7423	1.7388
Cr203	0.0742	0.0648	0.0451	0.0851	0.0643	0.0278	0.0855	0.0401	0.0732
Total	97.9774	97.8002	97.4987	97.9554	97.3542	98.3221	97.4151	98.1381	97.7649
Cations	(calculated on the basis of 23 O)								
Si	6.3478	6.3400	6.3268	6.3137	6.3164	6.3259	6.3133	6.3535	6.3474
Ti	0.1505	0.1507	0.1646	0.1667	0.0772	0.1500	0.1630	0.1241	0.1393
Al	2.1085	2.1088	2.1286	2.1334	2.1809	2.1393	2.1111	2.1063	2.0965
Fe	2.4137	2.4080	2.4000	2.4224	2.4330	2.4182	2.4119	2.4291	2.4175
Mn	0.1000	0.1022	0.1030	0.1091	0.1035	0.0982	0.1055	0.1009	0.0966
Mg	1.9942	2.0022	1.9867	1.9602	2.0570	1.9969	2.0149	2.0162	2.0211
Ca	1.8928	1.9139	1.9024	1.9095	1.9548	1.8935	1.9022	1.8982	1.8978
Na	0.5385	0.5266	0.5362	0.5427	0.4587	0.5326	0.5474	0.5415	0.5569
K	0.3414	0.3314	0.3283	0.3335	0.3275	0.3323	0.3451	0.3405	0.3410
Total	15.8874	15.8838	15.8766	15.8911	15.9090	15.8870	15.9144	15.9102	15.9141

Table B.3: Amphibole analyses

Sample	33D_hbl_19	33D_hbl_20	33D_hbl_21	33D_hbl_22	33D_hbl_23	33D_hbl_24	33E_ARIV_4	33E_HBL1_2	33E_HBL1_3
No.	90	91	92	93	94	95	117	146	147
Wt.%									
SiO2	41.5644	41.2514	40.4709	40.8769	41.3286	40.2802	40.4859	40.9405	40.9106
TiO2	1.4268	1.0434	1.2725	1.3777	1.4966	1.4723	1.2162	1.3235	0.9029
Al2O3	11.6394	11.6673	11.7743	11.5965	11.7211	12.0142	11.8367	11.4626	11.772
FeO	18.9959	18.2462	18.8351	19.052	18.8488	19.2673	19.3064	19.2732	19.1715
MnO	0.8304	0.7958	0.7162	0.7938	0.7909	0.7701	0.7267	0.8251	0.828
MgO	8.7863	9.1655	8.6249	8.5369	8.6084	8.1432	8.3398	8.5057	8.6919
CaO	11.4273	11.7756	11.464	11.52	11.6326	11.5462	11.3689	11.2542	11.2518
Na2O	1.8076	1.637	1.7765	1.7753	1.7444	1.7476	1.7492	1.9427	1.8225
K2O	1.74	1.5784	1.6996	1.7283	1.7294	1.7226	1.7185	1.7505	1.7443
Cr203	0.0288	0.0822	0	0.0173	0	0.0055	0.0153	0.0575	0.0688
Total	98.3795	97.4041	96.6341	97.2768	97.9009	96.9692	96.7637	97.3622	97.2057
Cations	(calculated on the basis of 23 O)								
Si	6.3460	6.3462	6.2905	6.3173	6.3306	6.2563	6.2963	6.3329	6.3314
Ti	0.1638	0.1207	0.1487	0.1601	0.1724	0.1720	0.1422	0.1540	0.1051
Al	2.0944	2.1155	2.1569	2.1122	2.1161	2.1993	2.1696	2.0897	2.1472
Fe	2.4255	2.3475	2.4483	2.4624	2.4146	2.5027	2.5110	2.4932	2.4813
Mn	0.1074	0.1037	0.0943	0.1039	0.1026	0.1013	0.0957	0.1081	0.1085
Mg	1.9996	2.1018	1.9982	1.9666	1.9655	1.8853	1.9333	1.9611	2.0051
Ca	1.8693	1.9410	1.9092	1.9075	1.9091	1.9215	1.8944	1.8652	1.8657
Na	0.5351	0.4883	0.5354	0.5320	0.5181	0.5263	0.5274	0.5826	0.5469
K	0.3389	0.3098	0.3370	0.3407	0.3379	0.3413	0.3409	0.3454	0.3444
Total	15.8800	15.8744	15.9185	15.9028	15.8669	15.9059	15.9109	15.9323	15.9356

Table B.4: Amphibole analyses

Sample	33D_hbl_19	33D_hbl_20	33D_hbl_21	33D_hbl_22	33D_hbl_23	33D_hbl_24	33E_ARIV_4	33E_HBL1_2	33E_HBL1_3
No.	90	91	92	93	94	95	117	146	147
Wt.%									
SiO2	41.5644	41.2514	40.4709	40.8769	41.3286	40.2802	40.4859	40.9405	40.9106
TiO2	1.4268	1.0434	1.2725	1.3777	1.4966	1.4723	1.2162	1.3235	0.9029
Al2O3	11.6394	11.6673	11.7743	11.5965	11.7211	12.0142	11.8367	11.4626	11.772
FeO	18.9959	18.2462	18.8351	19.052	18.8488	19.2673	19.3064	19.2732	19.1715
MnO	0.8304	0.7958	0.7162	0.7938	0.7909	0.7701	0.7267	0.8251	0.828
MgO	8.7863	9.1655	8.6249	8.5369	8.6084	8.1432	8.3398	8.5057	8.6919
CaO	11.4273	11.7756	11.464	11.52	11.6326	11.5462	11.3689	11.2542	11.2518
Na2O	1.8076	1.637	1.7765	1.7753	1.7444	1.7476	1.7492	1.9427	1.8225
K2O	1.74	1.5784	1.6996	1.7283	1.7294	1.7226	1.7185	1.7505	1.7443
Cr203	0.0288	0.0822	0	0.0173	0	0.0055	0.0153	0.0575	0.0688
Total	98.3795	97.4041	96.6341	97.2768	97.9009	96.9692	96.7637	97.3622	97.2057
Cations	(calculated on the basis of 23 O)								
Si	6.3460	6.3462	6.2905	6.3173	6.3306	6.2563	6.2963	6.3329	6.3314
Ti	0.1638	0.1207	0.1487	0.1601	0.1724	0.1720	0.1422	0.1540	0.1051
Al	2.0944	2.1155	2.1569	2.1122	2.1161	2.1993	2.1696	2.0897	2.1472
Fe	2.4255	2.3475	2.4483	2.4624	2.4146	2.5027	2.5110	2.4932	2.4813
Mn	0.1074	0.1037	0.0943	0.1039	0.1026	0.1013	0.0957	0.1081	0.1085
Mg	1.9996	2.1018	1.9982	1.9666	1.9655	1.8853	1.9333	1.9611	2.0051
Ca	1.8693	1.9410	1.9092	1.9075	1.9091	1.9215	1.8944	1.8652	1.8657
Na	0.5351	0.4883	0.5354	0.5320	0.5181	0.5263	0.5274	0.5826	0.5469
K	0.3389	0.3098	0.3370	0.3407	0.3379	0.3413	0.3409	0.3454	0.3444
Total	15.8800	15.8744	15.9185	15.9028	15.8669	15.9059	15.9109	15.9323	15.9356

Table B.5: Amphibole analyses

Sample	33E_HBL1_4	33E_HBL1_5	33E_HBL1_6	33E_HBL1_9	33E_HBL1_10	33E_HBL2_1	33E_HBL2_2	33E_HBL2_3	33E_HBL2_4
No.	148	149	150	153	154	155	156	157	158
Wt.%									
SiO2	40.770	41.016	41.215	40.750	40.631	40.947	40.997	40.842	40.743
TiO2	0.883	1.226	0.952	0.664	1.042	1.624	1.441	1.488	1.247
Al2O3	11.941	11.557	11.814	11.843	11.951	11.455	11.543	11.564	11.708
FeO	18.941	18.879	19.106	18.317	19.182	19.393	19.267	19.359	19.158
MnO	0.840	0.808	0.791	0.808	0.830	0.817	0.786	0.827	0.816
MgO	8.621	8.493	8.571	9.108	8.475	8.330	8.383	8.200	8.582
CaO	11.258	11.143	11.354	11.316	11.400	10.825	11.081	10.842	10.857
Na2O	1.750	1.867	1.822	1.766	1.564	2.018	2.001	2.020	1.835
K2O	1.681	1.741	1.700	1.675	1.842	1.789	1.804	1.752	1.746
Cr203	0.117	0.093	0.082	0.057	0.044	0.090	0.007	0.023	0.010
Total	96.8099	96.8454	97.4251	96.3424	97.0674	97.3298	97.3106	96.9158	96.7009
Cations	(calculated on the basis of 23 O)								
Si	6.3269	6.3612	6.3540	3.1770	6.3041	6.3373	6.3366	6.3398	6.3278
Ti	0.1030	0.1430	0.1104	0.0552	0.1215	0.1890	0.1675	0.1737	0.1457
Al	2.1840	2.1125	2.1466	1.4311	2.1853	2.0894	2.1027	2.1156	2.1431
Fe	2.4582	2.4487	2.4633	2.4633	2.4889	2.5101	2.4905	2.5131	2.4883
Mn	0.1104	0.1062	0.1033	0.1033	0.1091	0.1071	0.1029	0.1088	0.1073
Mg	1.9942	1.9634	1.9697	1.9697	1.9601	1.9218	1.9314	1.8972	1.9867
Ca	1.8718	1.8517	1.8755	1.8755	1.8951	1.7950	1.8351	1.8032	1.8066
Na	0.5265	0.5615	0.5447	1.0894	0.4705	0.6055	0.5996	0.6078	0.5527
K	0.3328	0.3443	0.3342	0.6685	0.3645	0.3533	0.3558	0.3470	0.3460
Total	15.9077	15.8925	15.9017	12.8329	15.8992	15.9084	15.9222	15.9061	15.9043

Appendix C

EMP data for Biotite

Table C.1: Biotite analyses

No.	14	15	16	42	43	64	65	66	67	105
Wt.%										
SiO2	34.66	36.73	36.54	36.34	35.89	37.91	43.06	38.22	36.49	36.47
TiO2	15.14	15.64	15.80	15.01	15.65	15.11	17.32	15.67	14.87	14.86
Al2O3	2.03	1.99	1.08	2.03	0.93	2.02	1.39	2.24	2.52	2.67
FeO	17.96	15.92	17.06	16.61	17.09	16.32	13.91	15.55	16.23	18.17
MnO	0.52	0.38	0.44	0.45	0.42	0.52	0.54	0.50	0.57	0.49
MgO	14.12	12.73	14.21	13.25	14.46	13.32	10.88	13.01	12.96	12.01
CaO	0.07	0.05	0.04	0.04	0.09	0.06	0.03	0.06	0.03	0.00
Na2O	0.04	0.02	0.03	0.01	0.02	0.03	0.16	0.05	0.04	0.04
K2O	7.14	8.67	8.73	9.20	8.13	9.25	10.56	9.86	9.41	9.46
Cr203	0.00	0.00	0.00	0.00	0.00	0.04	0.01	0.03	0.06	0.00
Total	91.66	92.13	93.93	92.95	92.67	94.60	97.92	95.24	93.25	94.22
Cations	Pfu (22 oxygen)									
Si	6.015	5.806	6.399	3.200	5.822	5.730	5.715	5.828	6.013	5.749
Ti	1.742	1.763	1.582	0.791	1.828	1.814	1.860	1.756	1.710	1.815
Al	0.352	0.448	0.383	0.255	0.400	0.445	0.333	0.450	0.539	0.384
Fe	1.905	2.081	1.764	1.764	2.100	2.274	2.333	2.233	2.136	2.281
Mn	0.043	0.043	0.031	0.031	0.051	0.059	0.063	0.053	0.049	0.069
Mg	3.088	3.153	2.857	2.857	2.979	2.961	3.032	2.872	2.572	3.016
Ca	0.028	0.019	0.000	0.000	0.017	0.008	0.014	0.014	0.004	0.004
Na	0.076	0.015	0.030	0.061	0.028	0.014	0.011	0.034	0.020	0.011
K	1.711	1.772	1.565	3.130	1.876	1.874	1.803	1.935	1.948	1.843
Total	14.960	15.100	14.626	12.089	15.102	15.178	15.165	15.175	14.991	15.172

Table C.2: Biotite analyses

Sample	33D_hbl_35	33E_ARIV_1	33E_ARIV_2	33E_ARIV_3	33E_ARIV_6	33E_ARV_1	33E_ARV_2	33E_ARV_3	33E_HBL1_7	33E_HBL2_5
No.	106	114	115	116	119	130	131	132	151	159
Wt.%										
SiO2	34.66	36.73	36.54	36.34	35.89	37.91	43.06	38.22	36.49	36.47
TiO2	15.14	15.64	15.80	15.01	15.65	15.11	17.32	15.67	14.87	14.86
Al2O3	2.03	1.99	1.08	2.03	0.93	2.02	1.39	2.24	2.52	2.67
FeO	17.96	15.92	17.06	16.61	17.09	16.32	13.91	15.55	16.23	18.17
MnO	0.52	0.38	0.44	0.45	0.42	0.52	0.54	0.50	0.57	0.49
MgO	14.12	12.73	14.21	13.25	14.46	13.32	10.88	13.01	12.96	12.01
CaO	0.07	0.05	0.04	0.04	0.09	0.06	0.03	0.06	0.03	0.00
Na2O	0.04	0.02	0.03	0.01	0.02	0.03	0.16	0.05	0.04	0.04
K2O	7.14	8.67	8.73	9.20	8.13	9.25	10.56	9.86	9.41	9.46
Cr203	0.00	0.00	0.00	0.00	0.00	0.04	0.01	0.03	0.06	0.00
Total	91.66	92.13	93.93	92.95	92.67	94.60	97.92	95.24	93.25	94.22
Cations										
Si	5.572	5.825	5.733	5.760	5.702	5.872	6.322	5.872	5.766	5.748
Ti	1.830	1.865	1.865	1.789	1.870	1.760	1.912	1.810	1.767	1.761
Al	0.384	0.373	0.199	0.380	0.175	0.369	0.240	0.406	0.468	0.496
Fe	2.415	2.112	2.239	2.202	2.271	2.114	1.708	1.998	2.144	2.395
Mn	0.070	0.051	0.059	0.060	0.056	0.068	0.067	0.065	0.076	0.065
Mg	3.383	3.009	3.323	3.130	3.424	3.075	2.380	2.980	3.053	2.821
Ca	0.012	0.008	0.006	0.006	0.015	0.010	0.004	0.009	0.005	0.000
Na	0.011	0.006	0.010	0.004	0.007	0.009	0.047	0.015	0.011	0.013
K	1.463	1.755	1.748	1.859	1.647	1.827	1.978	1.932	1.897	1.902
Total	15.143	15.003	15.182	15.192	15.167	15.102	14.659	15.088	15.188	15.201

Table C.3: Biotite analyses

Sample	33E_HBL2_6	33E_Bt_1	33E_Bt_2	33E_Bt_3	33E_Bt_4	33E_Bt_5	33E_Bt_6	33E_Bt_7	33E_Bt_8	33E_Bt_9
No.	160	170	171	172	173	174	175	176	177	178
Wt.%										
SiO2	33.13	36.29	36.39	36.13	36.33	34.97	36.63	38.80	36.30	36.62
TiO2	15.25	15.14	14.91	14.38	15.18	15.31	15.25	15.77	14.47	14.99
Al2O3	1.93	3.53	3.37	2.61	3.41	2.81	3.11	3.01	3.03	2.96
FeO	19.90	19.82	19.09	19.38	18.08	18.67	17.26	16.41	18.30	16.70
MnO	0.46	0.53	0.50	0.52	0.50	0.43	0.47	0.44	0.57	0.43
MgO	14.20	10.72	10.97	11.08	11.09	12.61	11.90	11.26	10.96	11.99
CaO	0.09	0.11	0.03	0.05	0.02	0.03	0.03	0.03	0.02	0.03
Na2O	0.02	0.03	0.04	0.01	0.04	0.02	0.08	0.08	0.05	0.04
K2O	5.31	9.46	9.62	9.25	9.67	7.82	9.72	10.19	9.06	9.57
Cr203	0.00	0.06	0.07	0.07	0.06	0.05	0.02	0.06	0.06	0.00
Total	90.29	95.73	95.04	93.55	94.54	92.77	94.70	96.12	92.98	93.54
Cations										
Si	5.427	5.671	5.714	5.776	5.717	5.585	5.733	5.923	5.800	5.780
Ti	1.878	1.780	1.761	1.729	1.796	1.839	1.795	1.811	1.739	1.779
Al	0.373	0.650	0.624	0.492	0.633	0.528	0.573	0.542	0.571	0.551
Fe	2.726	2.591	2.507	2.591	2.378	2.494	2.259	2.095	2.445	2.204
Mn	0.064	0.070	0.067	0.071	0.067	0.059	0.062	0.058	0.077	0.058
Mg	3.467	2.497	2.566	2.640	2.600	3.002	2.777	2.561	2.611	2.821
Ca	0.015	0.019	0.005	0.008	0.004	0.006	0.005	0.004	0.003	0.005
Na	0.006	0.008	0.011	0.003	0.012	0.006	0.024	0.023	0.016	0.011
K	1.110	1.886	1.927	1.886	1.940	1.592	1.941	1.983	1.847	1.926
Total	15.067	15.171	15.182	15.194	15.147	15.111	15.168	14.999	15.108	15.134

Table C.4: Biotite analyses

Sample	33E_Bt_10	33E_Bt_11	33E_Bt_12	33E_Bt_13	33E_Bt_14
No.	179	180	181	182	183
Wt.%					
SiO2	36.39	36.36	35.77	36.57	36.84
TiO2	15.22	14.93	15.25	14.94	14.96
Al2O3	3.14	3.16	3.52	2.76	3.86
FeO	17.45	17.70	17.99	17.80	17.21
MnO	0.43	0.47	0.49	0.53	0.49
MgO	12.23	11.85	11.87	12.07	11.62
CaO	0.04	0.05	0.08	0.04	0.05
Na2O	0.02	0.04	0.03	0.03	0.03
K2O	9.45	9.41	9.04	9.45	9.87
Cr203	0.04	0.06	0.06	0.07	0.03
Total	94.53	94.08	94.16	94.28	94.97
Cations					
Si	5.699	5.725	5.632	5.751	5.728
Ti	1.792	1.767	1.806	1.767	1.749
Al	0.579	0.587	0.653	0.511	0.707
Fe	2.286	2.331	2.369	2.341	2.238
Mn	0.057	0.062	0.065	0.070	0.064
Mg	2.855	2.782	2.785	2.828	2.693
Ca	0.006	0.009	0.013	0.007	0.008
Na	0.007	0.012	0.011	0.009	0.009
K	1.887	1.891	1.815	1.895	1.957
Total	15.167	15.166	15.149	15.178	15.152

Appendix D.1
Bulk Rock Sample - AR 1 Ultramylonite

T°C	^{39}Ar(mV)	^{39}Ar(%)	AGE (Ma)±1σ	% ATM	^{37}Ar/^{39}Ar	^{36}Ar/^{40}Ar	^{39}Ar/^{40}Ar	% IIC
650	200.7	11.5	972.6 ± 4.6	10.1	0.4	0.000345	0.003186	0.03
750	90.7	5.2	1205 ± 4.9	1	0.21	0.000036	0.002639	0.01
775	114.1	6.5	1210.3 ± 5.6	1.3	0.21	0.000045	0.002616	0.01
800	129.1	7.4	1209 ± 5.5	1	0.23	0.000037	0.002626	0.02
825	105.9	6.1	1199.7 ± 4.6	1.1	0.29	0.00004	0.002652	0.02
850	86.7	4.9	1181.7 ± 4.9	1.2	0.45	0.00004	0.002707	0.03
875	78.8	4.5	1165.7 ± 4.7	1.3	0.66	0.000044	0.002754	0.05
900	98.7	5.6	1187.1 ± 5	1.3	0.79	0.000046	0.002685	0.06
950	195.9	11.2	1184.1 ± 5	1.6	0.79	0.000057	0.002686	0.06
1000	359.2	20.6	1180.2 ± 4.7	1.7	0.92	0.000057	0.002698	0.07
1050	166.5	9.5	1167.6 ± 18.3	2.34	1.6	0.000081	0.002718	0.13
1100	47.8	2.7	1435.1 ± 6.3	5.4	5.3	0.000183	0.001972	0.42
1150	47.2	2.7	1684.4 ± 6.7	5.7	6.37	0.000193	0.001548	0.49
1200	3	0.1	2322.7 ± 17.4	34.8	1.36	0.001178	0.000629	0.09
1250	3.9	0.2	2394.9 ± 17.9	32.4	1.62	0.001098	0.000617	0.11
1300	7.9	0.4	1948.7 ± 17.8	39	1.75	0.001322	0.000794	0.13
1325	0.5	0	2278.7 ± 131	80.1	0.74	0.002711	0.000198	0.05

TOTAL GAS AGE = 1198.1 ± 9.8 Ma

J = .002536 ± 2.536E-05

^{37}Ar/^{39}Ar, ^{36}Ar/^{40}Ar AND ^{39}Ar/^{40}Ar ARE CORRECTED FOR MASS SPECTROMETER DISCRIMINATION, INTERFERING ISOTOPES AND SYSTEM BLANKS

% IIC - INTERFERING ISOTOPES CORRECTION

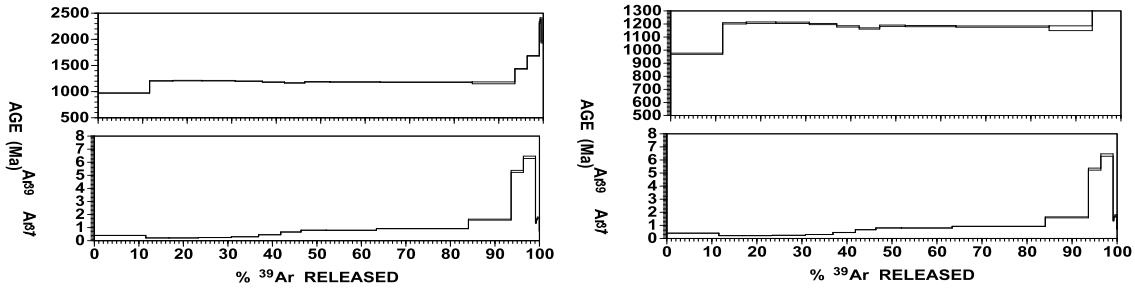

Appendix D.2
Bulk Rock Sample - AR 3 Mylonite

T°C	^{39}Ar(mV)	^{39}Ar(%)	AGE (Ma)±1σ	% ATM	^{37}Ar/^{39}Ar	^{36}Ar/^{40}Ar	^{39}Ar/^{40}Ar	% IIC
550	91.6	2	626.3 ± 2.6	2.1	0.1	0.000071	0.006007	0.01
600	230.2	5.1	647.8 ± 2.8	1	0.09	0.000036	0.005833	0.01
650	510.8	11.4	694.7 ± 2.9	0.4	0.08	0.000015	0.005397	0
700	585.4	13.1	788 ± 3.5	1.9	0.08	0.000064	0.004561	0
750	563	12.6	858.9 ± 3.8	0.2	0.1	0.000007	0.004167	0.01
800	483.7	10.8	883.1 ± 3.7	0.2	0.14	0.000007	0.004024	0.01
850	412.3	9.2	802.8 ± 3.6	0.4	0.21	0.000014	0.004525	0.02
900	466.4	10.4	764.7 ± 3.3	0.2	0.26	0.000009	0.004812	0.02
950	517	11.6	867.9 ± 3.7	0.2	0.31	0.000008	0.004112	0.03
1000	347.6	7.8	1014.5 ± 4.3	0.3	0.53	0.000013	0.003361	0.04
1050	142.6	3.2	1203.5 ± 4.6	0.1	0.81	0.000005	0.00268	0.06
1100	48.8	1	1719.6 ± 9.5	0.8	1.81	0.000028	0.001584	0.13
1150	32.4	0.7	2317.1 ± 7.9	1.2	3.32	0.000043	0.000962	0.24
1200	5.9	0.1	3235.6 ± 19	5.1	4.73	0.000175	0.000481	0.32
1250	2.9	0	3396 ± 34.8	7.2	6.47	0.000245	0.000424	0.44
1300	2.3	0	3468.8 ± 73.1	15	7.44	0.000508	0.00037	0.5
1320	0.3	0	39.4 ± 51	25.1	0	0.000849	0.086366	0

TOTAL GAS AGE = 872.5 ± 7.2 Ma

J = .002548 ± 2.548E-05

^{37}Ar/^{39}Ar, ^{36}Ar/^{40}Ar AND ^{39}Ar/^{40}Ar ARE CORRECTED FOR MASS SPECTROMETER DISCRIMINATION, INTERFERING ISOTOPES AND SYSTEM BLANKS

% IIC - INTERFERING ISOTOPES CORRECTION

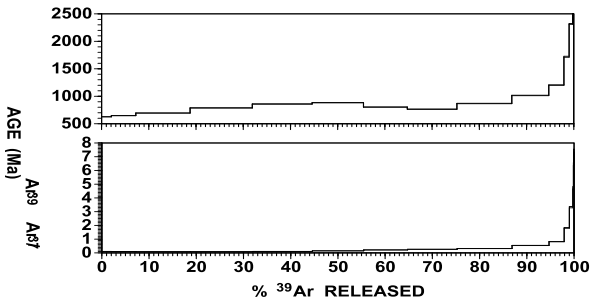

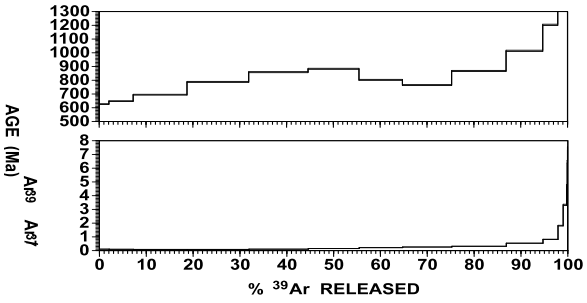

Appendix D.3
Bulk Rock Sample - AR 4 Mylonite

T°C	^{39}Ar(mV)	^{39}Ar(%)	AGE (Ma)±1σ	% ATM	^{37}Ar/^{39}Ar	^{36}Ar/^{40}Ar	^{39}Ar/^{40}Ar	% IIC
600	157.9	6.5	833.8 ± 75.8	0.7	0.09	0.000023	0.004313	0
650	376.4	15.5	677.8 ± 2.9	0.4	0.07	0.000015	0.00557	0
700	377.3	15.5	773.2 ± 3.6	4.4	0.08	0.000151	0.004556	0
750	396.3	16.3	816.6 ± 3.4	0.1	0.1	0.000005	0.00445	0
800	247.1	10.2	771.6 ± 3.2	0.2	0.16	0.000009	0.004768	0.01
850	199.2	8.2	735.8 ± 3.1	0.4	0.2	0.000015	0.005045	0.02
900	217.5	8.9	776.8 ± 3.2	0.5	0.2	0.000018	0.004716	0.02
950	179.7	7.4	836.1 ± 3.4	0.5	0.24	0.000019	0.004304	0.02
1000	101.4	4.1	881.4 ± 3.7	0.8	0.36	0.000027	0.004017	0.03
1050	54.8	2.2	938.4 ± 4.1	1	0.46	0.000036	0.003699	0.04
1100	30.8	1.2	1053.9 ± 4.4	1.6	0.67	0.000057	0.003161	0.06
1150	25	1	1177.4 ± 5.3	2.3	0.69	0.000079	0.002707	0.05
1200	18.5	0.7	1249.3 ± 5.7	3.3	0.69	0.000115	0.002468	0.05
1250	10.7	0.4	1404.6 ± 9.7	8.9	1.17	0.000302	0.001972	0.09
1300	19.6	0.8	1066 ± 5.9	11.3	0.41	0.000383	0.002809	0.03
1320	7	0.2	1313.8 ± 12	21.1	2.82	0.000714	0.001879	0.23

TOTAL GAS AGE = 800.7 ± 12.1 Ma

J = .002553 ± 2.553E-05

^{37}Ar/^{39}Ar, ^{36}Ar/^{40}Ar AND ^{39}Ar/^{40}Ar ARE CORRECTED FOR MASS SPECTROMETER DISCRIMINATION, INTERFERING ISOTOPES AND SYSTEM BLANKS

% IIC - INTERFERING ISOTOPES CORRECTION

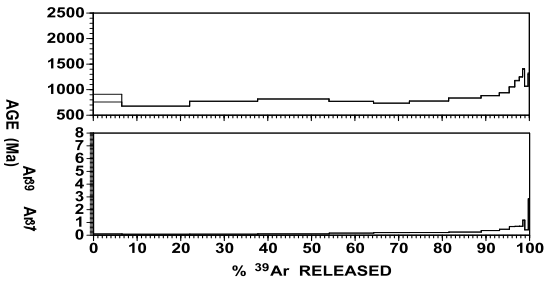

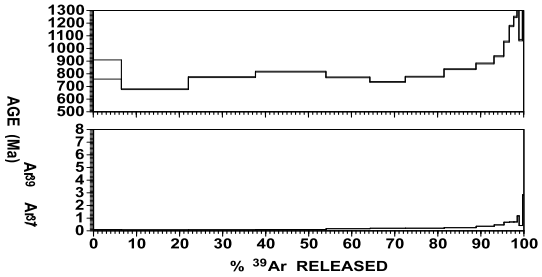

Appendix D.4
Bulk Rock Sample - AR 5 Mylonite

T°C	^{39}Ar(mV)	^{39}Ar(%)	AGE (Ma)±1σ	% ATM	^{37}Ar/^{39}Ar	^{36}Ar/^{40}Ar	^{39}Ar/^{40}Ar	% IIC
550	45.2	1.6	613.8 ± 2.7	1.7	0.17	0.000059	0.006194	0.01
600	161.3	5.8	609.4 ± 2.6	1	0.09	0.000034	0.006292	0.01
650	373.7	13.4	664.8 ± 3.5	0.5	0.08	0.000017	0.005705	0
700	414	14.8	752 ± 3.4	3.3	0.07	0.000114	0.004773	0
750	374.8	13.4	805.6 ± 3.4	0.3	0.08	0.00001	0.004524	0
800	304.1	10.9	779 ± 3.3	0.2	0.13	0.000008	0.004719	0.01
850	276.4	9.9	718.3 ± 3	0.3	0.17	0.000012	0.005205	0.01
900	274.1	9.8	737.1 ± 3.1	0.4	0.19	0.000013	0.005042	0.02
950	277.4	9.9	832.4 ± 3.4	0.3	0.29	0.000011	0.004343	0.02
1000	154.1	5.5	899.1 ± 3.6	0.4	0.63	0.000015	0.003937	0.05
1050	72.4	2.6	981.2 ± 4	0.6	1.31	0.000023	0.003511	0.12
1100	18.7	0.6	1172.5 ± 6.5	2	1.4	0.00007	0.002733	0.12
1150	12.8	0.4	1329.4 ± 6	3.4	2.29	0.000118	0.002263	0.18
1200	4.7	0.1	1517.4 ± 13	7	3.05	0.000239	0.0018	0.24
1250	13.3	0.4	1337.8 ± 8.9	14.7	1.81	0.000498	0.001982	0.14
1300	0.9	0	1822.4 ± 89	35.1	3.98	0.001188	0.000949	0.3
1320	0.8	0	1632 ± 135	45.3	7.56	0.001536	0.000948	0.59

TOTAL GAS AGE = 771.1 ± 6.6 Ma

J = .002556 ± 2.556E-05

^{37}Ar/^{39}Ar, ^{36}Ar/^{40}Ar AND ^{39}Ar/^{40}Ar ARE CORRECTED FOR MASS SPECTROMETER DISCRIMINATION, INTERFERING ISOTOPES AND SYSTEM BLANKS

% IIC - INTERFERING ISOTOPES CORRECTION

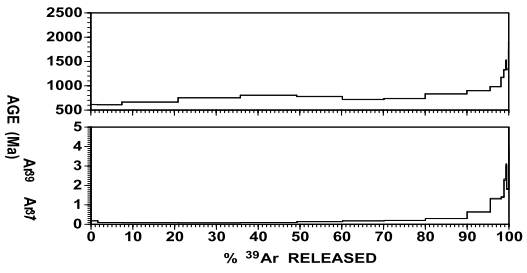

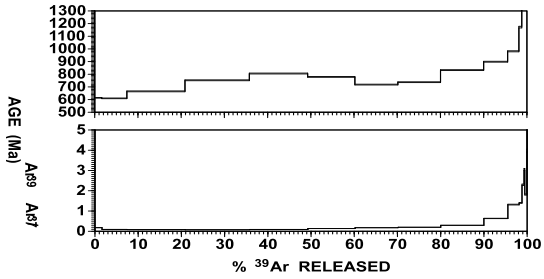

Appendix D.5
FELSIC CONCENTRATE ARGON SUMMARY

T°C	^{39}Ar(mV)	^{39}Ar(%)	AGE (Ma)±1σ	% ATM	$^{37}Ar/^{39}Ar$	$^{36}Ar/^{40}Ar$	$^{39}Ar/^{40}Ar$	% IIC
550	80.5	0.8	647.6 ± 2.8	0.6	0.14	0.00002	0.005901	0.01
600	260.7	2.9	819.1 ± 3.3	0.4	0.25	0.000016	0.00444	0.02
650	486.8	5.4	785.8 ± 3.3	0.3	0.17	0.000011	0.004681	0.01
700	661.1	7.3	755 ± 3.2	2	0.04	0.000068	0.004834	0
750	704.5	7.8	768.1 ± 3.2	0.2	0.03	0.000007	0.004821	0
800	612.4	6.8	800.6 ± 3.3	0.2	0.03	0.000009	0.004578	0
850	538	5.9	832.7 ± 3.6	0.2	0.03	0.000007	0.004361	0
900	542.4	6	887.5 ± 3.7	0.2	0.02	0.000008	0.004024	0
950	651.8	7.2	953.4 ± 3.9	0.2	0.02	0.000008	0.003672	0
1000	720.6	8	1047.7 ± 4.3	0.3	0.02	0.000011	0.003245	0
1050	804	8.9	1126.3 ± 4.4	0.3	0.03	0.000013	0.002946	0
1100	812.9	9	1262.8 ± 4.9	0.3	0.04	0.000013	0.002519	0
1150	1196.6	13.3	1349.8 ± 5.1	0.4	0.02	0.000015	0.002293	0
1200	740.4	8.2	1305.3 ± 4.9	0.4	0.01	0.000014	0.002404	0
1250	169.1	1.8	1650.9 ± 6.2	4.5	0.12	0.000153	0.001635	0
1300	0.6	0	3003.6 ± 92.1	19.8	0.58	0.000671	0.000479	0.04
1325	0.9	0	3502 ± 130	14.4	1.02	0.000489	0.000367	0.07

TOTAL GAS AGE = 1049.8 ± 8.3 Ma

J = .002565 ± 2.565E-05

$^{37}Ar/^{39}Ar$, $^{36}Ar/^{40}Ar$ AND $^{39}Ar/^{40}Ar$ ARE CORRECTED FOR MASS SPECTROMETER DISCRIMINATION, INTERFERING ISOTOPES AND SYSTEM BLANKS

% IIC - INTERFERING ISOTOPES CORRECTION

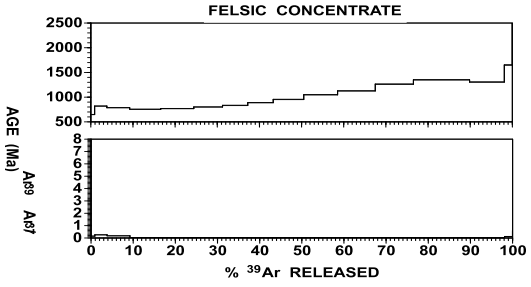

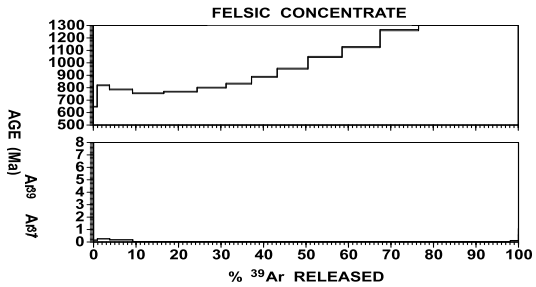

Appendix D.6
HORNBLENDE ARGON SUMMARY

T°C	^{39}Ar(mV)	^{39}Ar(%)	AGE (Ma)±1σ	% ATM	^{37}Ar/^{39}Ar	^{36}Ar/^{40}Ar	^{39}Ar/^{40}Ar	% IIC
600	32.6	2.2	1421.8 ± 5.4	4.2	0.91	0.000142	0.002053	0.07
700	71.8	4.8	1076 ± 6.1	14.7	0.43	0.0005	0.002685	0.03
750	60.4	4.1	1071.1 ± 4.6	1.7	0.13	0.000058	0.003115	0.01
775	38.2	2.5	1056 ± 5.6	1.3	0.11	0.000046	0.003185	0.01
800	29.8	2	1070.1 ± 4.6	1.4	0.11	0.000048	0.003128	0
850	36.6	2.4	1090.1 ± 4.8	1.7	0.14	0.000057	0.003044	0.01
900	50.7	3.4	1093.8 ± 4.7	1.6	0.46	0.000056	0.003031	0.04
925	47.5	3.2	1088.9 ± 4.7	1.2	0.74	0.000041	0.003063	0.06
950	84.1	5.7	1060.8 ± 4.6	0.5	1.52	0.000019	0.003192	0.13
975	146.6	9.9	1033.2 ± 4.5	0.3	2.09	0.00001	0.003314	0.18
1000	205.8	13.9	1021.9 ± 4.5	0.1	2.33	0.000006	0.003366	0.21
1025	179.3	12.1	1025.5 ± 4.5	0.1	2.33	0.000004	0.003353	0.21
1050	255.9	17.3	1028.1 ± 4.5	0	2.5	0.000002	0.003344	0.22
1075	58.4	3.9	1077.4 ± 4.8	0.3	2.12	0.000011	0.003134	0.18
1100	49.8	3.3	1044.5 ± 44	0.4	2.26	0.000015	0.003262	0.2
1150	80.7	5.4	1097.5 ± 4.7	0.4	2.47	0.000015	0.003054	0.21
1200	23.4	1.5	1204.5 ± 6.6	1.7	1.84	0.00006	0.002658	0.15
1250	17.4	1.1	1197.4 ± 27.2	7.3	1.86	0.000247	0.002528	0.15
1300	1.4	0	2286.7 ± 73.8	13.8	1.99	0.000467	0.000867	0.14
1325	2.4	0.1	2337.2 ± 107	10.5	2.82	0.000357	0.000866	0.2

TOTAL GAS AGE = 1066.7 ± 9 Ma

J = .002571 ± 2.571E-05

^{37}Ar/^{39}Ar, ^{36}Ar/^{40}Ar AND ^{39}Ar/^{40}Ar ARE CORRECTED FOR MASS SPECTROMETER DISCRIMINATION, INTERFERING ISOTOPES and SYSTEM BLANKS

% IIC - INTERFERING ISOTOPES CORRECTION